

**PHARMACOLOGICAL OPTIMIZATION OF THE  
ANTIHYPERTENSIVE AND VASORELAXANT  
EFFECTS OF A POLYHERBAL TRADITIONAL  
CHINESE MEDICINE EXTRACT BASED ON  
ORTHOGONAL STIMULUS-RESPONSE  
COMPATIBILITY APPROACH.**

**LOH YEAN CHUN**

**UNIVERSITI SAINS MALAYSIA**

**2017**

**PHARMACOLOGICAL OPTIMIZATION OF THE  
ANTIHYPERTENSIVE AND VASORELAXANT  
EFFECTS OF A POLYHERBAL TRADITIONAL  
CHINESE MEDICINE EXTRACT BASED ON  
ORTHOGONAL STIMULUS-RESPONSE  
COMPATIBILITY APPROACH**

by

**LOH YEAN CHUN**

**Thesis submitted in fulfillment of the requirements  
for the degree of  
Doctor of Philosophy**

**November 2017**

## ACKNOWLEDGEMENT

First and foremost, I would like to express my sincerest gratitude to my supervisor, Dr. Yam Mun Fei, who has given me this golden opportunity to conduct my research and relentlessly supported me throughout the whole study with his tremendous patience. This work would not have been possible without his guidance, support and encouragement. He strictly emphasised on the importance of accuracy and consistency of the result and taught me the value of honesty in scientific research. Under his guidance, I successfully overcame many difficulties and completed this research.

I gratefully acknowledge Tan Chu Shan, Ch'ng Yung Sing, Ng Chiew Hoong, and Yeap Zhao Qin who have guided and troubleshoot all the problems occurred during the studies with me. I would also like to thank my family and friends who had provided me at all times support, mentally and spiritually. Without their encouragement, motivation and love, I would not be able to consistently commit to this research exercise especially staying in the lab overnight.

Most importantly, I would like to acknowledge those SD rats and SHR<sub>s</sub> that were sacrificed in this research. Their scarification would contribute to a brighter future for the world. I am also grateful to the people who have ever helped me in completing my research, their contributions would be markedly remembered throughout my whole life.

## TABLE OF CONTENTS

Acknowledgement	ii
Table of Contents	iii
List of Tables	xi
List of Figures	xiv
List of Abbreviations	xxii
List of Symbols	xxviii
Abstrak	xxix
Abstract	xxx

### CHAPTER 1 - MICROENVIRONMENT OF THE BLOOD VESSELS IN VASCULAR TONE REGULATION

1.1	Introduction	1
1.2	Endothelium-Derived Relaxing Factors	2
1.2.1	Nitric Oxide	3
1.2.2	Prostacyclin	3
1.2.3	Endothelium-Derived Hyperpolarizing Factors	4
1.2.4	Hydrogen Sulfide	5
1.3	Enzyme-Linked Receptors	6
1.3.1	Soluble Guanylyl Cyclase	6
1.3.2	Serine-Threonine Protein Kinases	7
1.3.2(a)	Protein Kinase A	7
1.3.2(b)	Protein Kinase C	7
1.3.2(c)	Protein Kinase G	8
1.4	G Protein-Coupled Receptors	8
1.4.1	G <sub>q</sub> α Protein-Coupled Receptors	9
1.4.2	G <sub>i</sub> α Protein-Coupled Receptors	9
1.4.3	G <sub>s</sub> α Protein-Coupled Receptors	10
1.5	Channel-Linked Receptors	10

1.5.1	Potassium Channels	10
1.5.1(a)	Calcium-Activated K <sup>+</sup> Channel	11
1.5.1(b)	Voltage-Activated K <sup>+</sup> Channel	11
1.5.1(c)	Inwardly-Rectifying K <sup>+</sup> Channel	12
1.5.1(d)	ATP-Sensitive K <sup>+</sup> Channel	12
1.5.2	Calcium Channels	13
1.5.2(a)	Voltage-Operated Ca <sup>2+</sup> channel	13
1.5.2(b)	Receptor-Operated Ca <sup>2+</sup> channel	14
1.5.2(b)(i)	Inositol Triphosphate Receptor	14
1.5.2(b)(ii)	Ryanodine Receptor	15
1.5.2(b)(iii)	Store-Operated Ca <sup>2+</sup> channel	15
1.6	Problem Statements	17
1.7	Objectives	19

## **CHAPTER 2 – HERBAL AUTHENTICATION USING HIGH PERFORMANCE THIN LAYER CHROMATOGRAPHY AND TRI-STEP FOURIER TRANSFORM INFRARED SPECTROSCOPY**

2.1	Introduction	21
2.1.1	High Performance Thin Layer Chromatography	21
2.1.2	Tri-Step Fourier Transform Infrared Spectroscopy	22
2.2	Methodology	23
2.2.1	Herbs and Chemicals	23
2.2.2	High Performance Thin Layer Chromatography	24
2.2.2(a)	<i>Gastrodia elata</i>	25
2.2.2(b)	<i>Uncaria rhynchophylla</i>	26
2.2.2(c)	<i>Pueraria thomsonii</i>	26
2.2.2(d)	<i>Panax notoginseng</i>	26
2.2.2(e)	<i>Alisma orientale</i>	27
2.2.3	Tri-Step Fourier Transform Infrared	27
2.3	Results	28
2.3.1	<i>Gastrodia elata</i>	28

2.3.2	<i>Uncaria rhynchophylla</i>	33
2.3.3	<i>Pueraria thomsonii</i>	38
2.3.4	<i>Panax notoginseng</i>	43
2.3.5	<i>Alisma orientale</i>	48
2.4	Discussion	53
2.5	Conclusion	54

### **CHAPTER 3 – *IN VITRO* VASODILATORY EFFECT SCREENING AND CHARACTERIZATION OF FIVE HERBAL EXTRACTS**

3.1	Introduction	55
3.2	Methodology	56
3.2.1	Herbs and Chemicals	56
3.2.2	Herbal Extracts Preparation	56
3.2.3	Animals and Aortic Rings Preparation	57
3.2.4	Vascular Response to Herbal Extracts on PE Pre-Contracted Aortic Rings	58
3.2.5	Marker Compounds Characterization of Herbal Extracts by Using HPTLC	59
3.2.6	Characterization of the Chemical Constituents in Herbal Extracts by Using Tri-Step FTIR	59
3.2.7	Statistical Analysis	59
3.3	Results	59
3.3.1	Vasodilatory Effects of Herbal Extracts	59
3.3.2	Fingerprints Determination of Herbal Extracts	63
3.3.2(a)	<i>Gastrodia elata</i>	63
	3.3.2(a)(i) HPTLC	64
	3.3.2(a)(ii) Tri-Step FTIR	66
3.3.2(b)	<i>Uncaria rhynchophylla</i>	69
	3.3.2(b)(i) HPTLC	70
	3.3.2(b)(ii) Tri-Step FTIR	72
3.3.2(c)	<i>Pueraria thomsonii</i>	75

	3.3.2(c)(i)	HPTLC	76
	3.3.2(c)(ii)	Tri-Step FTIR	78
3.3.2(d)	<i>Panax notoginseng</i>		81
	3.3.2(d)(i)	HPTLC	82
	3.3.2(d)(ii)	Tri-Step FTIR	84
3.3.2(e)	<i>Alisma orientale</i>		87
	3.3.2(e)(i)	HPTLC	88
	3.3.2(e)(ii)	Tri-Step FTIR	90
3.4	Discussion		93
3.5	Conclusion		98

#### **CHAPTER 4 – MECHANISM ACTIONS OF *UNCARIA RHYNCHOPHYLLA* AND *PANAX NOTOGINSENG* FOR VASODILATORY EFFECTS**

4.1	Introduction		100
4.2	Methodology		103
4.2.1	Herbs and Chemicals		103
4.2.2	Herbal Extracts Preparation		103
4.2.3	Animals and Aortic Rings Preparation		103
4.2.4	Vascular Responses to UR95 and PN95 on PE Pre-Contracted Aortic Rings		104
4.2.5	Vasodilatory Effects of UR95 and PN95 in Endothelium- Denuded Aortic Rings		104
4.2.6	Vascular Responses of UR95 and PN95 on KCl Pre-Contracted Aortic Rings		104
4.2.7	The Roles of EDRFs in Vascular Responses of UR95 and PN95		105
4.2.8	The Roles of GPCRs in Vascular Responses of UR95 and PN95		105
4.2.9	The Roles of Channel-Linked Receptors in Vascular Responses of UR95 and PN95		106
4.2.9(a)	Roles of K <sup>+</sup> Channels		106
4.2.9(b)	Roles of Ca <sup>2+</sup> Channels		106
	4.2.9(b)(i)	Investigation on VOCC	106

	4.2.9(b)(ii) Investigation on IP <sub>3</sub> R	107
	4.2.10 Statistical Analysis	108
4.3	Results	108
	4.3.1 Primary Screening on Vascular Responses	108
	4.3.1(a) UR95	108
	4.3.1(b) PN95	110
	4.3.2 Roles of EDRFs and NO-Signaling Cascade in Vascular Response	112
	4.3.2(a) UR95	112
	4.3.2(b) PN95	114
	4.3.3 Roles of GPCRs in Vascular Response	116
	4.3.3(a) UR95	116
	4.3.3(b) PN95	118
	4.3.4 Roles of Potassium Channels in Vascular Response	119
	4.3.4(a) UR95	119
	4.3.4(b) PN95	121
	4.3.5 Roles of Calcium Channels in Vascular Response	125
	4.3.5(a) UR95	125
	4.3.5(b) PN95	128
4.4	Discussion	132
	4.4.1 UR95	132
	4.4.2 PN95	136
4.5	Conclusion	139

## **CHAPTER 5 - ORTHOGONAL STIMULUS-RESPONSE COMPATIBILITY GROUP STUDIES OF FIVE HERBS**

5.1	Introduction	140
5.2	Methodology	141
	5.2.1 Herbs and Chemicals	141
	5.2.2 Herbal Extracts Preparation	141
	5.2.3 Animals and Aortic Rings Preparation	141

5.2.4	Orthogonal Stimulus-Response Compatibility Group Studies	142
5.2.5	Preparation of Five Herbs using Different Solvents and Extraction Methods Following the F1 Ratio	142
5.2.6	Marker Compounds Characterization of F1 and Its Derivatives by using HPTLC	143
5.2.7	Characterization of Chemical Constituents in F1 and Its Derivatives by using Tri-Step FTIR	143
5.2.8	Statistical Analysis	144
5.3	Results	144
5.3.1	Orthogonal Stimulus-Response Compatibility Group Studies	144
5.3.2	Vasodilatory Effects of F1 and Its Derivatives	149
5.3.3	Marker Compounds Determination in F1 and Its Derivatives by using HPTLC	152
5.3.3(a)	Isorhynchophylline and Rhynchophylline	152
5.3.3(b)	Puerarin	154
5.3.3(c)	Ginsenosides Rg1 and Rb1	157
5.3.3(d)	Alisol B Acetate	160
5.3.4	Characterization of Chemical Constituents in F1 and Its Derivatives by using Tri-Step FTIR	163
5.4	Discussion	169
5.5	Conclusion	174

**CHAPTER 6 - OVERVIEW ON MECHANISM OF ACTIONS OF F1-2 FOR  
VASODILATORY EFFECTS AND *IN VIVO*  
ANTIHYPERTENSIVE STUDY WITH TOXICITY TEST**

6.1	Introduction	175
6.2	Methodology	176
6.2.1	Herbs and Chemicals	176
6.2.2	F1-2 Preparation	176
6.2.3	Animals Model	176
6.2.4	Aortic Rings Preparation	176

6.2.5	Vascular Response to F1-2 on PE Pre-Contracted Aortic Rings	177
6.2.6	Vasodilatory Effect of F1-2 in Endothelium-Denuded Aortic Rings	177
6.2.7	Vascular Response of F1-2 on KCl Pre-Contracted Aortic Rings	177
6.2.8	The Roles of EDRFs in Vascular Response of F1-2	177
6.2.9	The Roles of GPCRs in Vascular Response of F1-2	177
6.2.10	The Roles of Channel-Linked Receptors in Vascular Response of F1-2	178
6.2.10(a)	Roles of K <sup>+</sup> Channels	178
6.2.10(b)	Roles of Ca <sup>2+</sup> Channels	178
	6.2.10(b)(i) Investigation on VOCC	178
	6.2.10(b)(ii) Investigation on IP <sub>3</sub> R	178
6.2.11	Preparation of F1-2 and Propranolol and Orally Administration	179
6.2.12	Measurement of SBP, DBP, and MAP	179
6.2.13	Collection of Blood Samples	180
6.2.14	Clinical Biochemistry and Hematological Tests	180
6.2.15	Statistical Analysis	181
6.3	Results	181
6.3.1	Primary Screening on Vascular Response of F1-2	181
6.3.2	Roles of EDRFs and NO-Signaling Cascade in Vascular Response of F1-2	183
6.3.3	Roles of GPCRs in Vascular Response of F1-2	185
6.3.4	Roles of Potassium Channels in Vascular Response of F1-2	187
6.3.5	Roles of Calcium Channels in Vascular Response of F1-2	190
6.3.6	Measurements of SBP, DBP, and MAP on F1-2-Treated SHR <sub>s</sub>	193
6.3.7	Toxicity Tests	195
	6.3.7(a) Body Weight	195
	6.3.7(b) Clinical Biochemistry and Hematological Tests	196
6.4	Discussion	199
6.4.1	Mechanism of Actions of F1-2 for Vasodilatory Effects	199
6.4.2	Antihypertensive Effects of F1-2 in SHR <sub>s</sub>	203

6.4.3	Clinical Biochemistry and Hematological Tests	204
6.5	Conclusion	204

## **CHAPTER 7 - CONCLUSION**

<b>REFERENCES</b>	208
-------------------	-----

## **APPENDICES**

## **LIST OF PUBLICATIONS**

## LIST OF TABLES

		<b>Page</b>
Table 2.1	HPTLC quantitative summary of gastrodin contents in raw and standard herbs of <i>G. elata</i> .	30
Table 2.2	The 1D-IR spectra absorption peaks detected and characterization in standard and raw herbs of <i>G. elata</i> .	32
Table 2.3	HPTLC quantitative summary of isorhynchophylline and rhynchophylline contents in raw and standard herbs of <i>U. rhynchophylla</i> .	35
Table 2.4	The 1D-IR spectra absorption peaks detected and characterization in standard and raw herbs of <i>U. rhynchophylla</i> .	37
Table 2.5	HPTLC quantitative summary of puerarin contents in raw and standard herbs of <i>P. thomsonii</i> .	40
Table 2.6	The 1D-IR spectra absorption peaks detected and characterization in standard herb of <i>P. lobata</i> and raw herbs of <i>P. thomsonii</i> .	42
Table 2.7	HPTLC quantitative summary of ginsenoside Rg1 and ginsenoside Rb1 contents in raw and standard herbs of <i>P. notoginseng</i> .	45
Table 2.8	The 1D-IR spectra absorption peaks detected and characterization in standard and raw herbs of <i>P. notoginseng</i> .	47
Table 2.9	HPTLC quantitative summary of alisol b acetate contents in raw and standard herbs of <i>A. orientale</i> .	50
Table 2.10	The 1D-IR spectra absorption peaks detected and characterization in standard and raw herbs of <i>A. orientale</i> .	52
Table 3.1	The EC <sub>50</sub> and R <sub>max</sub> values obtained from the cumulative concentration-response curves of different extracts of <i>G. elata</i> , <i>U. rhynchophylla</i> , <i>P. thomsonii</i> , <i>P. notoginseng</i> , and <i>A. orientale</i> , respectively.	62
Table 3.2	HPTLC quantitative summary of gastrodin contents in 95% ethanolic, 50% ethanolic, and distilled water extracts of <i>G. elata</i> .	65
Table 3.3	HPTLC quantitative summary of isorhynchophylline and rhynchophylline contents in 95% ethanolic, 50% ethanolic, and distilled water extracts of <i>U. rhynchophylla</i> .	71

Table 3.4	HPTLC quantitative summary of puerarin contents in 95% ethanolic, 50% ethanolic, and distilled water extracts of <i>P. thomsonii</i> .	77
Table 3.5	HPTLC quantitative summary of ginsenosides Rg1 and Rb1 contents in 95% ethanolic, 50% ethanolic, and distilled water extracts of <i>P. notoginseng</i> .	83
Table 3.6	HPTLC quantitative summary of alisol b acetate contents in 95% ethanolic, 50% ethanolic, and distilled water extracts of <i>A. orientale</i> .	89
Table 4.1	EC <sub>50</sub> values and R <sub>max</sub> values on UR95 induced vasodilation in the presence of different antagonists.	123
Table 4.2	EC <sub>50</sub> values and R <sub>max</sub> values on PN95 induced vasodilation in the presence of different antagonists.	124
Table 4.3	Comparison of C <sub>max</sub> values among different treatments on calcium channels mechanism studies in UR95.	128
Table 4.4	Comparison of C <sub>max</sub> values among different treatments on calcium channels mechanism studies in PN95.	131
Table 5.1	The effective concentration selected from cumulative concentration-response curves of GE50, UR95, PT95, PN95, and AO50 for orthogonal stimulus-response compatibility groups studies.	145
Table 5.2	Orthogonal stimulus-response compatibility group studies.	146
Table 5.3	Average relaxation of aortic rings obtained from orthogonal stimulus-response compatibility groups studies.	147
Table 5.4	Confirmation test on optimum combination ratio of GE50, UR95, PT95, PN95, and AO50 in exerting strongest vasodilatory effects.	147
Table 5.5	The EC <sub>50</sub> and R <sub>max</sub> values of F1 and its derivatives.	151
Table 5.6	HPTLC quantitative summary of isorhynchophylline and rhynchophylline contents in F1 and its derivatives.	154
Table 5.7	HPTLC quantitative summary of puerarin contents in F1 and its derivatives.	157
Table 5.8	HPTLC quantitative summary of ginsenoside Rg1 contents in F1	159

	and its derivatives.	
Table 5.9	HPTLC quantitative summary of ginsenoside Rb1 contents in F1 and its derivatives.	160
Table 5.10	HPTLC quantitative summary of alisol b acetate contents in F1 and its derivatives.	162
Table 5.11	The 1D-IR spectra peaks characterization of F1 and its derivatives.	165
Table 6.1	Significance of $EC_{50}$ values and comparison of $R_{max}$ values obtained from the cumulative concentration-response curves under different pre-treatments in vasodilatory effect of F1-2.	189
Table 6.2	Comparison of $C_{max}$ values among different treatments on calcium channels mechanism studies in F1-2.	192
Table 6.3	Clinical biochemistry test results of SHRs blood samples after 28 days of oral administration with F1-2 (experimental groups), propranolol (positive control), and distilled water (negative control).	197
Table 6.4	Hematological test results of SHRs blood samples after 28 days of oral administration with F1-2 (experimental groups), propranolol (positive control), and distilled water (negative control).	198

## LIST OF FIGURES

		<b>Page</b>
Figure 1.1	Overall signaling mechanism pathways that happen in vascular endothelium and vascular smooth muscle cells which mediate vascular tone regulation.	16
Figure 2.1	The derivatized HPTLC plate examined under ultraviolet light at wavelength of (a) 366 nm, (b) 254 nm, and (c) white light for (i) gastrodin, (ii) <i>G. elata</i> raw herb, (iii) <i>G. elata</i> standard herb, with $R_f$ scale provided at both sides.	29
Figure 2.2	Representative 1D-IR spectra of <i>G. elata</i> (i) standard herb, and (ii) raw herb in wavelength ranging between 4000-400 $\text{cm}^{-1}$ .	31
Figure 2.3	The developed HPTLC plate examined under ultraviolet light at wavelength of (a) 366 nm, and (b) 254 nm, for (i) isorhynchophylline, (ii) rhynchophylline (iii) <i>U. rhynchophylla</i> standard herb, and (iv) <i>U. rhynchophylla</i> raw herb, with $R_f$ scale provided at both sides.	34
Figure 2.4	Representative 1D-IR spectra of <i>U. rhynchophylla</i> (i) standard herb, and (ii) raw herb in wavelength ranging between 4000-400 $\text{cm}^{-1}$ .	36
Figure 2.5	The (a, b) developed and (c, d) derivatized HPTLC plate examined under ultraviolet light at wavelength of (a) 366 nm, and (b) 254 nm, for (i) 1 mg/ml of puerarin, (ii) <i>P. thomsonii</i> standard herb, (iii) <i>P. thomsonii</i> raw herb, with $R_f$ scale provided at both sides.	39
Figure 2.6	Representative 1D-IR spectra of <i>P. lobata</i> (i) standard herb, and <i>P. thomsonii</i> (ii) raw herb in wavelength ranging between 4000-400 $\text{cm}^{-1}$ .	41
Figure 2.7	The derivatized HPTLC plate examined under ultraviolet light at wavelength of (a) 366 nm, (b) 254 nm, and (c) white light for (i) ginsenoside Rg1, (ii) ginsenoside Rb1 (iii) <i>P. notoginseng</i> standard herb, and (iv) <i>P. notoginseng</i> raw herb, with $R_f$ scale provided at both sides.	44
Figure 2.8	Representative 1D-IR spectra of <i>P. notoginseng</i> (i) standard herb, and (ii) raw herb in wavelength ranging between 4000-400 $\text{cm}^{-1}$ .	46
Figure 2.9	The derivatized HPTLC plate examined under ultraviolet light at wavelength of (a) 366 nm, (b) 254 nm, and (c) white light for (i)	49

alisol b acetate (ii) *A. orientale* standard herb and (iii) *A. orientale* raw herb with  $R_f$  scale provided at both sides.

Figure 2.10	Representative 1D-IR spectra of <i>A. orientale</i> (i) standard herb, and (ii) raw herb in wavelength ranging between 4000-400 $\text{cm}^{-1}$ .	51
Figure 3.1	The cumulative concentration-response curves of vasodilatory effects resulted from (a) GE95, GE50, and GEW, (b) UR95, UR50, and URW, (c) PT95, PT50, and PTW, (d) PN95, PN50, and PNW, (e) AO95, AO50, and AOW on 1 $\mu\text{M}$ PE pre-contracted isolated endothelium-intact SD rat aortic rings (n=8).	61
Figure 3.2	The derivatized HPTLC plate examined under ultraviolet light at wavelength of (a) 366 nm, (b) 254 nm, and (c) white light for (i) gastrodin, (ii) 95% ethanolic extracts (GE95), (iii) 50% ethanolic extract (GE50), (iv) distilled water extract (GEW) of <i>G. elata</i> , with $R_f$ scale provided at both sides.	64
Figure 3.3	Representative (a) 1D-IR and (b) SD-IR spectra of (i) 95% ethanolic (GE95), (ii) 50% ethanolic (GE50), and (iii) distilled water (GEW) extracts of <i>G. elata</i> in wavelength ranging between 4000-400 $\text{cm}^{-1}$ and 1800-800 $\text{cm}^{-1}$ , respectively.	66
Figure 3.4	The (i) autopeak, (ii) 2D-IR, and (iii) 3D-IR of (a) 95% ethanolic (GE95), (b) 50% ethanolic (GE50), and (c) distilled water (GEW) extracts of <i>G. elata</i> in the wavelength ranging between 1150-875 $\text{cm}^{-1}$ .	67
Figure 3.5	The (i) autopeak, (ii) 2D-IR, and (iii) 3D-IR of (a) 95% ethanolic (GE95), (b) 50% ethanolic (GE50), and (c) distilled water (GEW) extracts of <i>G. elata</i> in the wavelength ranging between 1520-1160 $\text{cm}^{-1}$ .	68
Figure 3.6	The developed HPTLC plate examined under ultraviolet light at wavelength of (a) 366 nm, and (b) 254 nm for (i) isorhynchophylline, (ii) rhynchophylline, (iii) 95% ethanolic extracts (UR95), (iv) 50% ethanolic extract (UR50), and (v) distilled water extract (URW) of <i>U. rhynchophylla</i> , with $R_f$ scale provided at both sides.	70
Figure 3.7	Representative (a) 1D-IR and (b) SD-IR spectra of (i) 95% ethanolic (UR95), (ii) 50% ethanolic (UR50), and (iii) distilled water (URW) extracts of <i>U. rhynchophylla</i> in wavelength ranging between 4000-400 $\text{cm}^{-1}$ and 1800-750 $\text{cm}^{-1}$ , respectively.	72
Figure 3.8	The (i) autopeak, (ii) 2D-IR, and (iii) 3D-IR of (a) 95% ethanolic (UR95), (b) 50% ethanolic (UR50), and (c) distilled water (URW)	73

	extracts of <i>U. rhynchophylla</i> in the wavelength ranging between 1100-850 $\text{cm}^{-1}$ .	
Figure 3.9	The (i) autopeak, (ii) 2D-IR, and (iii) 3D-IR of (a) 95% ethanolic (UR95), (b) 50% ethanolic (UR50), and (c) distilled water (URW) extracts of <i>U. rhynchophylla</i> in the wavelength ranging between 1500-1200 $\text{cm}^{-1}$ .	74
Figure 3.10	The (a, b) developed and (c, d) derivatized HPTLC plate examined under ultraviolet light at wavelength of (a, c) 366 nm, and (b, d) 254 nm for (i) puerarin, (ii) 95% ethanolic extracts (PT95), (iii) 50% ethanolic extract (PT50), and (iv) distilled water extract (PTW) of <i>P. thomsonii</i> , with $R_f$ scale provided at both sides.	76
Figure 3.11	Representative (a) 1D-IR and (b) SD-IR spectra of (i) 95% ethanolic (PT95), (ii) 50% ethanolic (PT50), and (iii) distilled water (PTW) extracts of <i>P. thomsonii</i> in wavelength ranging between 4000-400 $\text{cm}^{-1}$ and 1800-800 $\text{cm}^{-1}$ , respectively.	78
Figure 3.12	The (i) autopeak, (ii) 2D-IR, and (iii) 3D-IR of (a) 95% ethanolic (PT95), (b) 50% ethanolic (PT50), and (c) distilled water (PTW) extracts of <i>P. thomsonii</i> in the wavelength ranging between 1160-870 $\text{cm}^{-1}$ .	79
Figure 3.13	The (i) autopeak, (ii) 2D-IR, and (iii) 3D-IR of (a) 95% ethanolic (PT95), (b) 50% ethanolic (PT50), and (c) distilled water (PTW) extracts of <i>P. thomsonii</i> in the wavelength ranging between 1550-1160 $\text{cm}^{-1}$ .	80
Figure 3.14	The derivatized HPTLC plate examined under ultraviolet light at wavelength of (a) 366 nm, (b) 254 nm, and (c) white light for (i) ginsenoside Rg1, (ii) ginsenoside Rb1, (iii) 95% ethanolic extracts (PN95), (iv) 50% ethanolic extract (PN50), and (v) distilled water extract (PNW) of <i>P. notoginseng</i> , with $R_f$ scale provided at both sides.	82
Figure 3.15	Representative (a) 1D-IR and (b) SD-IR spectra of (i) 95% ethanolic (PN95), (ii) 50% ethanolic (PN50), and (iii) distilled water (PNW) extracts of <i>P. notoginseng</i> in wavelength ranging between 4000-400 $\text{cm}^{-1}$ and 1800-800 $\text{cm}^{-1}$ , respectively.	84
Figure 3.16	The (i) autopeak, (ii) 2D-IR, and (iii) 3D-IR of (a) 95% ethanolic (PN95), (b) 50% ethanolic (PN50), and (c) distilled water (PNW) extracts of <i>P. notoginseng</i> in the wavelength ranging between 1150-800 $\text{cm}^{-1}$ .	85
Figure 3.17	The (i) autopeak, (ii) 2D-IR, and (iii) 3D-IR of (a) 95% ethanolic	86

(PN95), (b) 50% ethanolic (PN50), and (c) distilled water (PNW) extracts of *P. notoginseng* in the wavelength ranging between 1800-1100  $\text{cm}^{-1}$ .

- Figure 3.18 The derivatized HPTLC plate examined under ultraviolet light at wavelength of (a) 366 nm, (b) 254 nm, and (c) white light for (i) alisol b acetate, (ii) 95% ethanolic extracts (AO95), (iii) 50% ethanolic extract (AO50), and (iv) distilled water extract (AOW) of *A. orientale*, with  $R_f$  scale provided at both sides. 88
- Figure 3.19 Representative (a) 1D-IR and (b) SD-IR spectra of (i) 95% ethanolic (AO95), (ii) 50% ethanolic (AO50), and (iii) distilled water (AOW) extracts of *A. orientale* in wavelength ranging between 4000-400  $\text{cm}^{-1}$  and 1800-800  $\text{cm}^{-1}$ , respectively. 90
- Figure 3.20 The (i) autopeak, (ii) 2D-IR, and (iii) 3D-IR of (a) 95% ethanolic (AO95), (b) 50% ethanolic (AO50), and (c) distilled water (AOW) extracts of *A. orientale* in the wavelength ranging between 1170-860  $\text{cm}^{-1}$ . 91
- Figure 3.21 The (i) autopeak, (ii) 2D-IR, and (iii) 3D-IR of (a) 95% ethanolic (AO95), (b) 50% ethanolic (AO50), and (c) distilled water (AOW) extracts of *A. orientale* in the wavelength ranging between 1520-1170  $\text{cm}^{-1}$ . 92
- Figure 4.1 The cumulative concentration-response curves of UR95 vasodilatory effects on PE-primed endothelium-intact aortic rings (control) compared to the vasodilatory effects exerted by UR95 on the PE-primed endothelium-denuded aortic rings or KCl-primed endothelium-intact aortic rings. (+E: endothelium-intact aortic rings; -E: endothelium-denuded aortic rings; \*:  $P < 0.05$ ; \*\*:  $P < 0.01$ ; \*\*\*:  $P < 0.001$ ;  $n = 8$ ). 109
- Figure 4.2 The cumulative concentration-response curves of PN95 vasodilatory effects on PE-primed endothelium-intact aortic rings (control) compared to the vasodilatory effects exerted by PN95 on the PE-primed endothelium-denuded aortic rings or KCl-primed endothelium-intact aortic rings. (+E: endothelium-intact aortic rings; -E: endothelium-denuded aortic rings; \*:  $P < 0.05$ ; \*\*:  $P < 0.01$ ; \*\*\*:  $P < 0.001$ ;  $n = 8$ ). 111
- Figure 4.3 The cumulative concentration-response curves of UR95 vasodilatory effects on PE-primed endothelium-intact aortic rings (control) compared to vasodilatory effects exerted by UR95 upon L-NAME, ODQ, MB, or indomethacin pre-treated PE-primed endothelium-intact aortic rings (+E: endothelium-intact aortic rings; \*:  $P < 0.05$ ; \*\*:  $P < 0.01$ ; \*\*\*:  $P < 0.001$ ;  $n = 8$ ). 113

Figure 4.4	The cumulative concentration-response curves of PN95 vasodilatory effects on PE-primed endothelium-intact aortic rings (control) compared to the vasodilatory effects exerted by PN95 upon L-NAME, ODQ, MB, or indomethacin pre-treated PE-primed endothelium-intact aortic rings (+E: endothelium-intact aortic rings; *: P<0.05; **: P<0.01; ***: P<0.001; n=8).	115
Figure 4.5	The cumulative concentration-response curves of UR95 vasodilatory effects on PE-primed endothelium-intact aortic rings (control) compared to the vasodilatory effects exerted by UR95 upon atropine or propranolol pre-treated PE-primed endothelium-intact aortic rings (+E: endothelium-intact aortic rings; *: P<0.05; **: P<0.01; n=8)	117
Figure 4.6	The cumulative concentration-response curves of PN95 vasodilatory effects on PE-primed endothelium-intact aortic rings (control) compared to the vasodilatory effects exerted by PN95 upon atropine or propranolol pre-treated PE-primed endothelium-intact aortic rings (+E: endothelium-intact aortic rings; *: P<0.05; ***: P<0.001; n=8).	118
Figure 4.7	The cumulative concentration-response curves of UR95 vasodilatory effects on PE-primed endothelium-intact aortic rings (control) compared to the vasodilatory effects exerted by UR95 upon TEA, glibenclamide, 4-AP, or BaCl <sub>2</sub> pre-treated PE-primed endothelium-intact aortic rings (+E: endothelium-intact aortic rings; *: P<0.05; **: P<0.01; ***: P<0.001; n=8)	120
Figure 4.8	The cumulative concentration-response curves of PN95 vasodilatory effects on PE-primed endothelium-intact aortic rings (control) compared to the vasodilatory effects exerted by PN95 upon TEA, glibenclamide, 4-AP, or BaCl <sub>2</sub> pre-treated PE-primed endothelium-intact aortic rings (+E: endothelium-intact aortic rings; *: P<0.05; **: P<0.01; ***: P<0.001; n=8).	122
Figure 4.9	(a) The vasoconstriction response-curves obtained from cumulative addition of CaCl <sub>2</sub> on untreated endothelium-intact aortic rings (control) compared to nifedipine (0.1, 0.3, and 1 μM) or UR95 (0.005, 0.02, and 0.08 mg/ml) pre-treated endothelium-intact aortic rings, (b) the vasoconstriction response induced by PE on untreated endothelium-denuded aortic rings (control) compared to 2-APB (100 μM) or UR95 (0.005, 0.02, and 0.08 mg/ml) pre-treated endothelium-denuded aortic rings (*: P<0.05; **: P<0.01; ***: P<0.001; n=8).	127

- Figure 4.10 (a) The vasoconstriction response-curves obtained from cumulative addition of  $\text{CaCl}_2$  on untreated endothelium-intact aortic rings (control) compared to nifedipine (0.1, 0.3, and 1  $\mu\text{M}$ ) or PN95 (0.005, 0.04, and 0.32 mg/ml) pre-treated endothelium-intact aortic rings, (b) the vasoconstriction response induced by PE on untreated endothelium-denuded aortic rings (control) compared to 2-APB (100  $\mu\text{M}$ ) or PN95 (0.005, 0.04, and 0.32 mg/ml) pre-treated endothelium-denuded aortic rings (\*:  $P < 0.05$ ; \*\*:  $P < 0.01$ ; \*\*\*:  $P < 0.001$ ;  $n=8$ ). 130
- Figure 5.1 Vasodilatory effects of F1 and F4 in cumulative concentration of 0.0025-1.2275 mg/ml on 1  $\mu\text{M}$  PE pre-contracted isolated endothelium-intact SD rat aortic rings ( $n=8$ ). F1: extracts GE50, UR95, PT95, PN95, and AO50 combined in EC: 0, 25, 20, 20, and 10, respectively. F4: extracts GE50, UR95, PT95, PN95, and AO50 combined in EC: 20, 15, 0, 20, and 10, respectively. The  $R_{\text{max}}$  values were compared among each other to ensure the efficacy of F1. 148
- Figure 5.2 Vasodilatory effects of F1, F1-1, F1-2, F1-3, F1-4, and F1-5 with cumulative concentration of 0.0025-0.3175 mg/ml on 1  $\mu\text{M}$  PE pre-contracted isolated endothelium-intact SD rat aortic rings ( $n=8$ ) (\*:  $P < 0.05$ , \*\*:  $P < 0.01$ , \*\*\*:  $P < 0.001$ ); F1-1: distilled water extract of five herbs using F1 ratio at 50  $^{\circ}\text{C}$ ; F1-2: 50% ethanolic extract of five herbs using F1 ratio at 50  $^{\circ}\text{C}$ ; F1-3: 95% ethanolic extract of five herbs using F1 ratio at 50  $^{\circ}\text{C}$ ; F1-4: total 95% of ethanolic extraction of *U. rhynchophylla*, *P. thomsonii*, and *P. notoginseng* (using F1 ratio) combined with AO50 (using F1 ratio) at 50  $^{\circ}\text{C}$ ; F1-5: distilled water extract of five herbs using F1 ratio at 100  $^{\circ}\text{C}$ ; The  $R_{\text{max}}$  values were compared among each other to determine the formula with the highest efficacy in terms of exerting vasodilatory effects. 150
- Figure 5.3 The developed HPTLC plate examined under ultraviolet light at wavelength of (a) 366 nm, and (b) 254 nm, for (i) isorhynchophylline, (ii) rhynchophylline, (iii) F1, (iv) F1-1, (v) F1-2, (vi) F1-3, (vii) F1-4, and (viii) F1-5, with  $R_f$  scale provided at both sides. 153
- Figure 5.4 The (a, b) developed and (c, d) derivatized HPTLC plate examined under ultraviolet light at wavelength of (a, c) 366 nm, and (b, d) 254 nm, for (i) puerarin, (ii) F1, (iii) F1-1, (iv) F1-2, (v) F1-3, (vi) F1-4, and (vii) F1-5, with  $R_f$  scale provided at both sides. 156
- Figure 5.5 The derivatized HPTLC plate examined under ultraviolet light at wavelength of (a) 366 nm, and (b) 254 nm, as well as (c) white light, for (i) ginsenoside Rg1 (ii) ginsenoside Rb1, (iii) F1, (iv) F1- 159

	1, (v) F1-2, (vi) F1-3, (vii) F1-4, and (viii) F1-5, with $R_f$ scale provided at both sides.	
Figure 5.6	The derivatized HPTLC plate examined under ultraviolet light at wavelength of (a) 366 nm, and (b) 254 nm, as well as (c) white light, for (i) alisol b acetate (ii) F1, (iii) F1-1, (iv) F1-2, (v) F1-3, (vi) F1-4, and (vii) F1-5, with $R_f$ scale provided at both sides.	162
Figure 5.7	Representative 1D-IR spectra of (i) F1, (ii) F1-1, (iii) F1-2, (iv) F1-3, (v) F1-4, and (vi) F1-5 in wavelength ranging among 4000-400 $\text{cm}^{-1}$ , respectively.	164
Figure 5.8	Representative SD-IR spectra of (i) F1, (ii) F1-1, (iii) F1-2, (iv) F1-3, (v) F1-4, and (vi) F1-5 in wavelength ranging among 1800-750 $\text{cm}^{-1}$ , respectively.	166
Figure 5.9	Representative autopeaks, 2D-IR, and 3D-IR spectra of (a) F1, (b) F1-1, (c) F1-2, (d) F1-3, (e) F1-4, and (f) F1-5 in wavelength ranging between 1600-850 $\text{cm}^{-1}$ .	168
Figure 6.1	The cumulative concentration-response curves of F1-2 vasodilatory effects on PE-primed endothelium-intact aortic rings (control) compared to the vasodilatory effects exerted by F1-2 on the PE-primed endothelium-denuded aortic rings or KCl-primed endothelium-intact aortic rings. (+E: endothelium-intact aortic rings; -E: endothelium-denuded aortic rings; *: $P<0.05$ ; **: $P<0.01$ ; ***: $P<0.001$ ; $n=8$ ).	182
Figure 6.2	The cumulative concentration-response curves of F1-2 vasodilatory effects on PE-primed endothelium-intact aortic rings (control) compared to vasodilatory effects exerted by F1-2 upon L-NAME, ODQ, MB, or indomethacin pre-treated PE-primed endothelium-intact aortic rings (+E: endothelium-intact aortic rings; *: $P<0.05$ ; **: $P<0.01$ ; ***: $P<0.001$ ; $n=8$ ).	184
Figure 6.3	The cumulative concentration-response curves of F1-2 vasodilatory effects on PE-primed endothelium-intact aortic rings (control) compared to the vasodilatory effects exerted by F1-2 upon atropine or propranolol pre-treated PE-primed endothelium-intact aortic rings (+E: endothelium-intact aortic rings; *: $P<0.05$ ; **: $P<0.01$ ; ***: $P<0.001$ ; $n=8$ ).	186
Figure 6.4	The cumulative concentration-response curves of F1-2 vasodilatory effects on PE-primed endothelium-intact aortic rings (control) compared to the vasodilatory effects exerted by F1-2 upon TEA, glibenclamide, 4-AP, or $\text{BaCl}_2$ pre-treated PE-primed endothelium-intact aortic rings (+E: endothelium-intact aortic	188

rings; \*: P<0.05; \*\*: P<0.01; \*\*\*: P<0.001; n=8).

- Figure 6.5 (a) The vasoconstriction response-curves obtained from cumulative addition of CaCl<sub>2</sub> on untreated endothelium-intact aortic rings (control) compared to nifedipine (0.1, 0.3, and 1 μM) or F1-2 (0.005, 0.02, and 0.08 mg/ml) pre-treated endothelium-intact aortic rings, (b) the vasoconstriction response induced by PE on untreated endothelium-denuded aortic rings (control) compared to 2-APB (100 μM) or F1-2 (0.005, 0.02, and 0.08 mg/ml) pre-treated endothelium-denuded aortic rings (\*: P<0.05; \*\*: P<0.01; \*\*\*: P<0.001; n=8). 191
- Figure 6.6 Effects of 0.97092 g/kg (high dose), 0.48546 g/kg (medium dose), and 0.24273 g/kg (small dose) of F1-2, and 80 mg/kg propranolol (positive control) on (a) systolic blood pressure (SBP), (b) diastolic blood pressure (DBP), and (c) mean arterial pressure (MAP) of SHRs during 28 days of orally administration and compared to the control group (\*: P<0.05; \*\*: P<0.01; \*\*\*: P<0.001; Mean±S.E.M.; n=6). 195
- Figure 6.7 The changes of body weight on 0.97092 g/kg (high dose), 0.48546 g/kg (medium dose), and 0.24273 g/kg (small dose) of F1-2-treated groups, and 80 mg/kg propranolol-treated group (positive control), as well as the untreated group of SHRs during the 28 days of orally administration (\*\*\*: P<0.001; Mean±S.E.M.; n=6). 196

## LIST OF ABBREVIATIONS

<b>1D-IR</b>	1D-Infrared
<b>2-APB</b>	2-Aminoethoxydiphenyl Borate
<b>2D-IR</b>	2D-Infrared
<b>4-AP</b>	4-Aminopyridine
<b>5-HT<sub>1D</sub></b>	5-Hydroxytryptamine 1D Receptor
<b>A/G</b>	Albumin/Globulin Ratio
<b>AA</b>	Arachidonic Acid
<b>AC</b>	Adenylyl Cyclase
<b>Ach</b>	Acetylcholine
<b>ADC 2</b>	Automatic Developing Chamber 2
<b>AHA</b>	American Heart Association
<b>Akt</b>	Protein Kinase B
<b>AlbP</b>	Albumin Protein
<b>ALP</b>	Alkaline Phosphatase
<b>ALT</b>	Alanine Aminotransferase
<b>AMP</b>	Adenosine Monophosphate
<b>AO50</b>	50% Ethanolic Extract Of <i>Alisma Orientale</i>
<b>AO95</b>	95% Ethanolic Extract Of <i>Alisma Orientale</i>
<b>AOW</b>	Distilled Water Extract Of <i>Alisma Orientale</i>
<b>AR</b>	Actual Relaxation
<b>ARASC</b>	Animal Research And Service Centre

<b>AST</b>	Aspartate Aminotransferase
<b>AT<sub>2</sub></b>	Angiotensin II Receptor Type 2
<b>ATP</b>	Adenosine Triphosphate
<b>ATS 4</b>	Automatic TLC Sampler 4
<b>AU</b>	Absorbance Units
<b>B<sub>2</sub></b>	Bradykinin Receptor 2
<b>BaCl<sub>2</sub></b>	Barium Chloride
<b>BiD</b>	Direct Bilirubin
<b>BiT</b>	Total Bilirubin
<b>BK<sub>ca</sub></b>	Big-Conductance Calcium-Activated Potassium Channels
<b>BP</b>	Blood Pressure
<b>BUSE</b>	Blood Urea Serum Electrolyte
<b>Ca<sup>2+</sup></b>	Calcium Ions
<b>CALCRL</b>	Calcitonin Receptor-Like Receptor
<b>cAMP</b>	Cyclic Adenosine Monophosphate
<b>CBS</b>	Cystathionine Beta Synthase
<b>cGMP</b>	Cyclic Guanosine Monophosphate
<b>CICR</b>	Calcium-Induced Calcium Release
<b>Cl<sup>-</sup></b>	Chloride Ions
<b>C<sub>max</sub></b>	Maximum Contraction
<b>CMC</b>	Carboxymethyl Cellulose
<b>COX</b>	Cyclooxygenases
<b>CSE</b>	Cystathionine Gamma-Lyase

<b>CYP</b>	Cytochrome P450
<b>DAG</b>	Diacylglycerol
<b>DMSO</b>	Dimethyl Sulfoxide
<b>EC<sub>50</sub></b>	Half Of Maximum Effective Concentration
<b>EDRFs</b>	Endothelium-Derived Relaxing Factors
<b>EETs</b>	Epoxyeicosatrienoic Acid
<b>EGTA</b>	Ethylene Glycol-bis(β-aminoethyl ether)-N,N,N',N'-tetraacetic Acid
<b>eNOS</b>	Endothelial Nitric Oxide Synthase
<b>ER</b>	Endoplasmic Reticulum
<b>ET<sub>B</sub>R</b>	Endothelin Receptor Type B
<b>FTIR</b>	Fourier Transform Infrared
<b>G protein</b>	Guanine Nucleotide-Binding Proteins
<b>GDP</b>	Guanosine Diphosphate
<b>GE50</b>	50% Ethanolic Extract of <i>Gastrodia Elata</i>
<b>GE95</b>	95% Ethanolic Extract of <i>Gastrodia Elata</i>
<b>GEF</b>	Guanine Nucleotide Exchange Factor
<b>GEW</b>	Distilled Water Extract of <i>Gastrodia Elata</i>
<b>GGT</b>	Gamma-Glutamyl Transferase
<b>GMP</b>	Guanosine Monophosphate
<b>GPCRs</b>	G Protein-Coupled Receptors
<b>GTP</b>	Guanosine Triphosphate
<b>H<sub>2</sub>S</b>	Hydrogen Sulfide
<b>HCT</b>	Hematocrit

<b>HGB</b>	Hemoglobin
<b>HPTLC</b>	High Performance Thin Layer Chromatography
<b>IK<sub>ca</sub></b>	Intermediate-Conductance Calcium-Activated Potassium Channel
<b>iNOS</b>	Inducible Nitric Oxide Synthase
<b>IP</b>	Prostacyclin Receptor
<b>IP<sub>3</sub></b>	Inositol Triphosphate
<b>IP<sub>3</sub>R</b>	Inositol Triphosphate Receptor
<b>JNC 7</b>	Seventh Report Of The Joint National Committee
<b>K<sup>+</sup></b>	Potassium Ions
<b>K<sub>ATP</sub></b>	ATP-Sensitive Potassium Channels
<b>KBr</b>	Potassium Bromide
<b>K<sub>ca</sub></b>	Calcium-Activated Potassium Channels
<b>K<sub>ir</sub></b>	Inwardly-Rectifying Potassium Channels
<b>Krebs'</b>	Krebs-Henseleit Solution
<b>K<sub>v</sub></b>	Voltage-Operated Potassium Channels
<b>LFT</b>	Liver Functional Test
<b>L-NAME</b>	L-N <sup>G</sup> -Nitro Arginine Methyl Ester
<b>M<sub>3</sub></b>	Muscarinic Acetylcholine Receptor 3
<b>MAP</b>	Mean Arterial Pressure
<b>MB</b>	Methylene Blue
<b>MCHC</b>	Mean Corpuscular Hemoglobin Concentration
<b>MCV</b>	Mean Cell Volume
<b>MLCK</b>	Myosin-Light-Chain Kinase

<b>MLCP</b>	Myosin-Light-Chain Phosphatase
<b>Na<sup>+</sup></b>	Sodium
<b>nNOS</b>	Neuronal Nitric Oxide Synthase
<b>NSAID</b>	Non-Steroidal Anti-Inflammation Drugs
<b>ODQ</b>	1H-[1,2,4] Oxadiazolo [4,3-a]Quinoxalin-1-One
<b>pD<sub>2</sub></b>	Negative Logarithm To Base 10 Of The EC50
<b>PDE</b>	Phosphodiesterase
<b>PE</b>	Phenylephrine
<b>PGH<sub>2</sub></b>	Prostaglandin H <sub>2</sub>
<b>PIP<sub>2</sub></b>	Phosphatidylinositol 4,5-Bisphosphate
<b>PKA</b>	Protein Kinase A
<b>PKC</b>	Protein Kinase C
<b>PKG</b>	Protein Kinase G
<b>PLA<sub>2</sub></b>	Phospholipase A <sub>2</sub>
<b>PLC</b>	Phospholipase C
<b>PLT</b>	Platelet
<b>PN50</b>	50% Ethanolic Extract Of <i>Panax Notoginseng</i>
<b>PN95</b>	95% Ethanolic Extract Of <i>Panax Notoginseng</i>
<b>PNW</b>	Distilled Water Extract Of <i>Panax Notoginseng</i>
<b>PT50</b>	50% Ethanolic Extract Of <i>Pueraria Thomsonii</i>
<b>PT95</b>	95% Ethanolic Extract Of <i>Pueraria Thomsonii</i>
<b>PTW</b>	Distilled Water Extract Of <i>Pueraria Thomsonii</i>
<b>RBC</b>	Red Blood Cell

<b>R<sub>f</sub></b>	Retention Factor
<b>RFT</b>	Renal Functional Test
<b>R<sub>max</sub></b>	Maximum relaxation
<b>ROCC</b>	Receptor-Operated Calcium Channel
<b>RyRs</b>	Ryanodine Receptor
<b>SD</b>	Standard Deviation
<b>SD-IR</b>	Second-Derivative Infrared
<b>SERCA</b>	Sacro/Endoplasmic Reticulum Ca <sup>2+</sup> -ATPase
<b>sGC</b>	Soluble Guanylyl Cyclase
<b>SHRs</b>	Spontaneous Hypertensive Rats
<b>SK<sub>ca</sub></b>	Small-Conductance Calcium-Activated Potassium Channels
<b>SR</b>	Sacroplasmic Reticulum
<b>TCM</b>	Traditional Chinese Medicine
<b>TP</b>	Total Protein
<b>TRPV<sub>4</sub></b>	Transient Receptor Potential Cation Channel Subfamily V
<b>TXA<sub>2</sub></b>	Thromboxane A <sub>2</sub>
<b>UR50</b>	50% Ethanolic Extract Of <i>Uncaria Rhynchophylla</i>
<b>UR95</b>	95% Ethanolic Extract Of <i>Uncaria Rhynchophylla</i>
<b>URW</b>	Distilled Water Extract Of <i>Uncaria Rhynchophylla</i>
<b>VOCC</b>	Voltage-Operated Calcium Channels
<b>VSMCs</b>	Vascular Smooth Muscle Cells
<b>WBC</b>	White Blood Cell
<b>WHO</b>	World Health Organization

## LIST OF SYMBOLS

%	percentage
°C	degree Celsius
$10^9/l$	$10^9$ cells per liter
$10^{12}/l$	$10^{12}$ cells per liter
$\mu\text{g/ml}$	microgram per liter
$\mu\text{l}$	microliter
$\mu\text{M}$	micromolar
$\mu\text{mol/l}$	micromole per liter
fl	femtoliter
g	gram
g/dl	gram per deciliter
g/l	gram per liter
mg	milligram
mg/ml	milligram per liter
mM	millimolar
mm	millimeter
mmHg	millimeter of mercury
mmol/l	millimole per liter
pg	picogram
rpm	rotation per minute
U/l	units per liter

**PENGOPTIMUMAN KESAN ANTIHIPERTENSIF DAN VASORELAKSAN  
SECARA FARMAKOLOGI BAGI EKSTRAK UBATAN TRADISIONAL CINA  
POLIHERBA BERDASARKAN PENDEKATAN KESERASIAN TINDAK  
BALAS RANGSANGAN ORTOGONAL**

**ABSTRAK**

Hipertensi merupakan salah satu masalah kesihatan yang utama dan berkaitan dengan pelbagai penyakit seiring dan komplikasi, kebanyakan komplikasi berlaku pada buah pinggang serta sistem kardiovaskular dan hal ini telah mendapat perhatian saintis di seluruh dunia kebelakangan ini. Walaupun terdapat ubat-ubatan antihipertensi sintetik di pasaran, efikasi yang rendah dalam kaedah monoterapi, serta kesan sampingan kerap dilaporkan. Oleh itu, kajian ini bertujuan mewujudkan satu formula antihipertensi baru dengan menggunakan teori gabungan sindromik-penyakit yang baharu daripada kaedah perubatan tradisional Cina (TCM). Pemilihan herba TCM untuk kajian ini iaitu *Gastrodia elata*, *Uncaria rhynchophylla*, *Pueraria thomsonii*, *Panax notoginseng*, dan *Alisma orientale* adalah berdasarkan keupayaan herba-herba ini dalam merawat tiga sindrom utama tekanan darah tinggi seperti api, pengekalan cecair kahak, dan sindrom-sindrom difisiensi. Keutuhan kelima-lima herba mentah telah disahkan oleh kromatografi lapisan nipis berprestasi tinggi (HPTLC) dan kaedah spektroskopi inframerah dengan teknik pembetulan Fourier tiga fasa (FTIR) sebagai pengesahan cap jari sebelum eksperimen. Kesan vasodilatori kesemua ekstrak telah disiasat dengan menggunakan asai *in vitro* cincin aortic terencil. Ekstrak etanolik 95% *U. rhynchophylla* (UR95), *P. thomsonii* (PT95), dan *P. notoginseng* (PN95), serta ekstrak etanolik 50% *G. elata* (GE50), dan *A. orientale* (AO50) didapati sebagai ekstrak yang

paling kuat dalam pendorongan kesan vasodilatori berbanding dengan ekstrak dalam pelarut lain. Oleh itu, ekstrak ini telah digunakan untuk kajian keserasian kumpulan ortogonal rangsangan-tindakan, dan nisbah yang terbaik (F1) didapati pada EC<sub>0</sub>, EC<sub>25</sub>, EC<sub>20</sub>, EC<sub>20</sub> dan EC<sub>10</sub> masing-masing adalah GE50 UR95, PT95, PN95, dan AO50. Selain itu, ekstrak (F1-2) lima herba mentah yang telah disediakan dalam nisbah F1 dan diekstrak dalam etanol sebanyak 50% seterusnya disahkan sebagai ekstrak yang paling kuat dalam pameran kesan vasodilatori berbanding dengan ekstrak yang lain melalui nilai EC<sub>50</sub> dan R<sub>max</sub> pada 0.028±0.005 mg/ml dan 101.71±3.64%. Kesan vasodilatori F1-2 adalah disebabkan tetapi bukan sahaja terhadap isorinkofilin, rinkohfilin, puerarin, ginsenosida Rg1 dan Rb1, serta asitat alisol b melalui NO/sGC/cGMP, adrinerjik-β<sub>2</sub> dan reseptor-M<sub>3</sub>, serta mekanisme rangkaian isyarat K<sub>ca</sub>, K<sub>v</sub>, K<sub>ir</sub>, K<sub>ATP</sub>, VOCC dan IP<sub>3</sub>R. Kesan antihipertensi F1-2 telah ditentukan dengan lebih lanjut secara *in vivo* selama 28 hari dengan penyuaapan sub-kronik dalam tikus hipertensi spontan (SHRs). Hasil kajian menunjukkan penurunan yang ketara dalam tekanan darah SHR berbanding dengan kumpulan kawalan bergantung kepada dos, manakala tidak menyebabkan apa-apa kesan sampingan di darah elektrolit urea serum, fungsi buah pinggang, fungsi hati, kiraan darah lengkap, dan kiraan pengkamiran tikus SHR walaupun sehingga dos yang tinggi (970.92 mg/kg) penyuaapan F1-2 dalam model haiwan. Secara muktamadnya, F1-2 dijumpai sebagai berjaya dan berpotensi sebagai ubat anti-hipertensi dalam penggunaan ke atas manusia pada masa hadapan.

**PHARMACOLOGICAL OPTIMIZATION OF THE ANTIHYPERTENSIVE  
AND VASORELAXANT EFFECTS OF A POLYHERBAL TRADITIONAL  
CHINESE MEDICINE EXTRACT BASED ON ORTHOGONAL STIMULUS-  
RESPONSE COMPATIBILITY APPROACH**

**ABSTRACT**

Hypertension is one of the major health concerns that are related to various concomitant diseases as well as complications that mainly occur in kidney and cardiovascular system and it has gained the attention of worldwide scientists in recent. Despite the availability of synthetic anti-hypertensive drugs in the market, the low efficacies in monotherapy, as well as adverse effects are frequently being reported. Hence, the current study decided to establish a new antihypertensive formula by applying a new syndromic-disease combination theory of traditional Chinese medicine (TCM). The selection of TCM herbs for current study which includes *Gastrodia elata*, *Uncaria rhynchophylla*, *Pueraria thomsonii*, *Panax notoginseng*, and *Alisma orientale* was based on their abilities to treat three main syndromes of hypertension such as fire, phlegm fluid retention, and deficiency syndromes. The authenticity of the five raw herbs was verified by high performance thin layer chromatography (HPTLC) and tri-step Fourier transform infrared (FTIR) fingerprints identification methods prior to the experiments. The vasodilatory effects of all extracts were investigated by using the *in vitro* isolated aortic rings assays. The 95% ethanolic extracts of *U. rhynchophylla* (UR95), *P. thomsonii* (PT95), and *P. notoginseng* (PN95), as well as 50% ethanolic extracts of *G. elata* (GE50), and *A. orientale* (AO50) were found as the most potent extracts for exerting vasodilatory effects compared to other solvent extracts. Hence,

these extracts were used for orthogonal stimulus-response compatibility group studies, and the best ratio (F1) was found at EC<sub>0</sub>, EC<sub>25</sub>, EC<sub>20</sub>, EC<sub>20</sub>, and EC<sub>10</sub> for GE50, UR95, PT95, PN95, and AO50, respectively. Moreover, the extract (F1-2) of five raw herbs which were prepared in F1 ratio and extracted in total by 50% ethanol was further confirmed as the most potent extract in exhibiting vasodilatory effects compared to any other extracts at EC<sub>50</sub> and R<sub>max</sub> values of  $0.028 \pm 0.005$  mg/ml and  $101.71 \pm 3.64\%$ , respectively. The vasodilatory effects of F1-2 were elicited by but not limited to isorhynchophylline, rhynchophylline, puerarin, ginsenosides Rg1 and Rb1, and alisol b acetate through NO/sGC/cGMP,  $\beta_2$ -adrenergic and M<sub>3</sub>-receptors, and also K<sub>ca</sub>, K<sub>v</sub>, K<sub>ir</sub>, K<sub>ATP</sub>, VOCC, and IP<sub>3</sub>R signaling mechanism pathways. The antihypertensive effects of F1-2 were further determined *in vivo* by 28 days sub-chronic oral administration in spontaneous hypertensive rats (SHRs). Results showed significant decrease of SHRs blood pressure compared to negative control in dose-dependent manner, whilst without causing any adverse effects in the blood urea serum electrolyte, renal function, liver function, full blood count, and differential count of the SHRs even until the high dose (970.92 mg/kg) of F1-2 administration. Conclusively, F1-2 was discovered to be a successful and could be a potentially useful antihypertensive drug for future use on humans.

## **CHAPTER 1**

### **MICROENVIRONMENT OF THE BLOOD VESSELS IN VASCULAR TONE REGULATION**

#### **1.1 Introduction**

Hypertension is a well-known “silent killer” and is one of the major risk factors of cardiovascular diseases. It is defined as persistently high blood pressure (BP) exerted against the wall of the arteries. There are approximately 13% of human populations in the earth suffering from hypertension and majority of them are from developing countries. In 2013, there was more than 32.7% of Malaysian aged  $\geq 18$  years old, and 43.5% of Malaysian aged  $\geq 30$  years old suffering from hypertension (MOH, 2013). The World Health Organization (WHO) has rated the hypertension as one of the most deadly causes of premature deaths worldwide. Hypertension is asymptomatic, it can live in anyone of us without causing any symptoms, and lead to concomitant diseases after many years, such as stroke.

Hypertension is categorized into several stages according to the American Heart Association (AHA) and Joint National Committee 7 (JNC 7). Normal BP stage has systolic pressure  $\leq 120$  mmHg and diastolic pressure  $\leq 80$  mmHg; pre-hypertension stage has systolic pressure ranging between 120-139 mmHg or diastolic pressure ranging between 80-89 mmHg; stage 1 hypertension has systolic pressure between 140-159 mmHg or diastolic pressure between 90-99 mmHg; and stage 2 hypertension has systolic pressure  $\geq 160$  mmHg or diastolic pressure  $\geq 100$  mmHg. In addition, a person with

systolic pressure of  $\geq 180$  mmHg or diastolic pressure  $\geq 110$  mmHg are considered as critical and should be treated immediately as medical emergency.

Generally, there are three types of blood vessels which includes the artery, vein, and capillary, they are responsible in transporting blood throughout the whole body. There are three layers present in artery and vein, where the outer most layer known as tunica adventitia, middle layer as tunica media, and innermost layer as tunica intima. Tunica media is rich of vascular smooth muscle cells (VSMCs), whereas tunica intima is composed of a thin layer of endothelial cells. Both the VSMCs and endothelium are the place where the vasomotors are located (Jakala et al., 2009, Yildiz et al., 2013). From the literatures, different parts of blood vessels were used by different researchers for vasculatures studies. However, based on the statistical analysis tabulated from 2010-2015, there were approximately 67% of the researches who recommend the use of aorta as the “golden tool” for pharmacological research in regards to vasculature, in order to minimize the orientation change of VSMCs and reduce the probability of causing damage to the endothelium (Loh et al., 2016). Generally, the vasomotors can cause the vascular tone to react in two ways such as vasodilation or vasoconstriction where both reactions are strictly dependent on the dominancy of the receptors present on the vascular endothelium and VSMCs as well as the interactions between their signals.

## **1.2 Endothelium-Derived Relaxing Factors (EDRFs)**

There are two well-characterized EDRFs present in endothelium such as nitric oxide (NO) and prostacyclin (PGI<sub>2</sub>). Additionally, the endothelium-derived hyperpolarizing factor (EDHF), and hydrogen sulfide (H<sub>2</sub>S) have been claimed to be one of the EDRFs as well recently.

### **1.2.1 Nitric oxide (NO)**

Generally, the NO can be produced by three isoform of NO synthase (NOS) such as neuronal NOS (nNOS), inducible NOS (iNOS), and endothelial NOS (eNOS). In endothelium, the increase in the concentration of the calcium in cytosol will enhance the formation of calcium-calmodulin complexes, which will activate the calmodulin-binding domain of the eNOS, and causes NO production. Other than that, the increase in hemodynamic shear stress, protein kinase A (PKA), and protein kinase B (Akt) in the blood vessel will induce the phosphorylation of the eNOS at Ser1179 site (Quillon et al., 2015, Zhao et al., 2015). Once the eNOS is activated, it will catalyze the breakdown of L-arginine into NO. Subsequently, NO will diffuse into adjacent VSMCs to stimulate the activity of the components down its signaling cascade such as soluble guanylyl cyclase (sGC), cyclic guanosine monophosphate (cGMP), and protein kinase G (PKG), hence resulting in vasodilation (Jakala et al., 2009, Moncada, 2007). The production of the NO can further stimulate the  $K_{ca}$  channels (Bolotina et al., 1994, Li et al., 1997) and voltage-activated  $K^+$  channels ( $K_v$ ) through the sGC-independent pathway (Yuan et al., 1996). Regarding the mechanism study, the selective antagonist of eNOS, L-N<sup>G</sup>-Nitro arginine methyl ester (L-NAME) is frequently used due to its low toxicity, and more solubility at neutral pH compared to other inhibitors (Balligand et al., 1993, Pfeiffer et al., 1996).

### **1.2.2 Prostacyclin (PGI<sub>2</sub>)**

It is also known as prostaglandin I<sub>2</sub>, and is well-known as one of the important EDRFs which is capable of inhibiting platelet aggregation. In endothelium, the precursor of the PGI<sub>2</sub> is arachidonic acid (AA) which ordinarily exists in the phospholipid bilayer of membranes. The AA will be released into the cytosol either catalyzed by

phospholipase A<sub>2</sub> (PLA<sub>2</sub>) or diacylglycerol (DAG) lipase by breaking down the phospholipid. The free mobile AA will be converted into prostaglandin H<sub>2</sub> (PGH<sub>2</sub>) by cyclooxygenase (COX). Subsequently, the prostacyclin synthase will catalyze the breakdown of PGH<sub>2</sub> into PGI<sub>2</sub>, whilst some of the PGH<sub>2</sub> is converted into thromboxane (TXA<sub>2</sub>) by thromboxane synthase. Both the TXA<sub>2</sub> and PGI<sub>2</sub> functions are physiologically antagonize. The PGI<sub>2</sub> will bind to the prostacyclin receptor (IP) which is located on the membrane of the VSMCs. IP is a G<sub>s</sub>α protein-coupled receptor, once the G<sub>s</sub>α protein is bound to guanosine triphosphate (GTP), the membrane-bound adenylyl cyclase (AC) will be stimulated to convert the adenosine triphosphate (ATP) into 3',5'-cyclic adenosine monophosphate (cAMP), which will then activate the PKA, and causes vasodilatory effects (Berumen et al., 2012, Nichols and Nichols, 2008). In the mechanism studies, the non-selective COX inhibitor, indomethacin which is a non-steroidal anti-inflammatory drug (NSAID) is frequently used compared to others such as ibuprofen, meclofenamic acid, and diclofenac. Indomethacin is preferred because it can bind rapidly to the COX with high-affinity, is time-dependent and has slow reversibility (Dannhardt and Kiefer, 2001, Smith et al., 2000).

### **1.2.3 Endothelium-derived hyperpolarizing factors (EDHFs)**

EDHFs were discovered when there were residual of endothelium-dependent relaxation observed even after the depletion of both NO and PGI<sub>2</sub> (Scotland et al., 2005, Wang, 2002). It is a kind of electrical signal that originated from the endothelium, which could subsequently induce the hyperpolarizing current in adjacent VSMC and cause vasodilatory effect. In vasculature, EDHF can be generated through various kinds of the reactions that happens between different biochemical components. For instance, part of the AA in the endothelium could be broken down into epoxyeicosatrienoic acids (EETs)

by cytochrome P450 (CYP) epoxygenase, at which the EETs could activate the small-conductance  $\text{Ca}^{2+}$ -activated  $\text{K}^+$  channels ( $\text{SK}_{\text{ca}}$ ) and intermediate-conductance  $\text{Ca}^{2+}$ -activated  $\text{K}^+$  channels ( $\text{IK}_{\text{ca}}$ ) which is located on the endothelium, hence causing the  $\text{K}^+$  ions efflux, and induce the hyperpolarizing current that will be passed onto the adjacent VSMCs via the myoendothelial gap junction, which was electrically-coupled between both endothelial cells and VSMCs, and ultimately causing the VSMCs hyperpolarization and relaxation. Furthermore, the EETs can activate the transient receptor potential vanilloid 4 (TRPV4) that is located on the endothelium to allow  $\text{Ca}^{2+}$  influx into the cytosol, and subsequently causes an increase of intracellular calcium concentration ( $\text{Ca}^{2+}$  spark) due to the calcium-induced calcium release (CICR) reaction when the influx cytosolic  $\text{Ca}^{2+}$  stimulates the ryanodine receptors (RyRs) that are located on the sarcoplasmic reticulum (SR). However, in terms of action potential, the efflux of  $\text{K}^+$  ions into the myoendothelial space leads to an increase in concentration of  $\text{K}^+$ , causing the activation of the inwardly-rectifying  $\text{K}^+$  channels ( $\text{K}_{\text{ir}}$ ) on the VSMCs to allow the influx of  $\text{K}^+$  ions back into the cytosol of VSMCs, and followed by efflux of  $\text{K}^+$  ions through the big-conductance  $\text{Ca}^{2+}$ -activated  $\text{K}^+$  channels ( $\text{BK}_{\text{ca}}$ ) to extracellular and causes hyperpolarization, resulting in vasodilatory effect (Pires et al., 2013, Quyyumi and Ozkor, 2006).

#### **1.2.4 Hydrogen sulfide ( $\text{H}_2\text{S}$ )**

$\text{H}_2\text{S}$  has a similar chemical profile as NO in vasculature. In the endothelium, the  $\text{H}_2\text{S}$  is produced from the L-cysteine which is catalyzed by cystathionine  $\gamma$ -lyase (CSE) and/or cystathionine  $\beta$ -synthase (CBS). The  $\text{H}_2\text{S}$  is capable of activating the  $\text{IK}_{\text{ca}}$  and  $\text{SK}_{\text{ca}}$  channels in endothelium, hence producing the hyperpolarizing current. Literatures stated that the production of  $\text{H}_2\text{S}$  could be increased at least two-fold in endothelium

when triggered by the VEGF and muscarinic receptors activation through the  $\text{Ca}^{2+}$ -calmodulin-dependent activation of the CSE (Coletta et al., 2012, Wang, 2009). Moreover,  $\text{H}_2\text{S}$  is diffusible into the adjacent VSMCs to inhibit the ATP from binding with ATP-sensitive  $\text{K}^+$  channels ( $\text{K}_{\text{ATP}}$ ), hence activating the channels and subsequently allowing the  $\text{K}^+$  efflux which results in hyperpolarization.  $\text{H}_2\text{S}$  is also capable of inhibiting the phosphodiesterase 5 (PDE5) from breaking down the cGMP, hence enhances the vasodilatory effects.

### **1.3 Enzyme-Linked Receptors**

These receptors can be called catalytic receptors which are located on the membrane. These receptors are functionally activated by catalytic enzymes and ligand-receptors. In vasculature, the guanylyl cyclase and serine-threonine protein kinases are the major enzyme-linked receptors that play the roles in vascular tone regulation.

#### **1.3.1 Soluble guanylyl cyclase (sGC)**

As aforementioned, the sGC is freely mobile in the cytosol of VSMCs which will be activated once the NO comes to bind with the heme group of sGC. Once the sGC is activated, it will cleave the GTP into cGMP, subsequently activates the PKG, and causes vasodilatory effect (Horowitz et al., 1996, Ko et al., 2008). The 1H-[1,2,4] oxadiazolo [4,3-a]quinoxalin-1-one (ODQ) is soluble in dimethyl sulfoxide (DMSO) and was reported to inhibit the sGC by oxidizing the heme group of the sGC (Moro et al., 1996, Olson et al., 1997, Schrammel et al., 1996) and it is more frequently being used compared to the other cGMP lowering agent, methylene blue (MB) (Kontos and Wei, 1993, Mayer et al., 1993).

### **1.3.2 Serine-threonine protein kinases**

It is basically a group of kinase enzymes that is functionally activated when bound to their respective secondary messengers, and subsequently phosphorylates the hydroxyl (OH) group of serine or threonine side chain of proteins which results in physiological effects. In vascular tone regulation, the protein kinases involved are PKA, PKC, and PKG.

#### **1.3.2(a) Protein kinase A (PKA)**

PKA is also known as the cAMP-dependent protein kinase which is functionally activated once bound with cAMP. Once bound with cAMP, its detaching catalytic subunits will phosphorylates the serine or threonine sites of its substrate proteins, and causes vasodilatory effect, whilst the cAMP will be broken down into adenosine monophosphate (AMP) by phosphodiesterase 3 (PDE3) (Bowen and Haslam, 1991). Regarding this mechanism study on cAMP-dependent PKA pathway, the Rp-cAMPs is commonly used due to its cell-permeability, resistance to PDE degradation as well as its selectivity towards PKA (Bouschet et al., 2003). Additionally, the selective inhibitor for PDE 3 that is commonly used is milrinone.

#### **1.3.2(b) Protein kinase C (PKC)**

In both vascular endothelium and VSMCs, the PKC will be activated by DAG and binds with  $Ca^{2+}$  ions at C1 and C2 domain, respectively (Huang, 1989). Once the PKC is activated, it will phosphorylate the serine or threonine sites of its substrate proteins, hence causes vasoconstriction. The most commonly used blockers for PKC is BIM due to its high permeability and selectivity.

### **1.3.2(c) Protein kinase G (PKG)**

As aforementioned, the PKG will be functionally activated once the cGMP binds to the regulatory units of the PKG without causing enzyme dissociation. After that, the activated catalytic units of the enzyme will phosphorylates the serine or threonine sites of its substrate proteins, and causes vasodilatory effect (Wall et al., 2003), whilst the cGMP will be broken down into guanosine monophosphate (GMP) which is catalyzed by PDE 5 (Paul and Snyder, 2012). The most commonly used cGMP-dependent PKG inhibitor is Rp-8-Br-PET cGMPs due to its high stability and the ability to block both PKG 1 and PKG 2 (Valtcheva et al., 2009). Additionally, the selective inhibitors for PDE 5 commonly used are sildenafil, dipyridamole, zaprinast and T-1032.

### **1.4 G Protein-Coupled Receptors (GPCRs)**

GPCRs are also known as the seven-transmembrane domain receptors which are functionally activated when bound to its ligands to transmit the signals from the outside of the cell into its interior. Generally, there are three types of guanine nucleotide binding protein (G protein) subunits such as  $G_{\alpha}$ ,  $G_{\beta}$ , and  $G_{\gamma}$  proteins, and the former is the one who plays the major role in vascular tone regulation which is further classified into at least three main sub-types such as  $G_{q\alpha}$ ,  $G_{i\alpha}$ , and  $G_{s\alpha}$ . The activation of the G protein will be initiated once the GPCRs bind to its ligand which subsequently causes the G protein temporary acting as guanine nucleotide exchange factor (GEF) by changing its conformation, and exchange its guanosine diphosphate (GDP) into GTP. Once bound with GTP, the G protein trimer will be dissociated into  $G_{\alpha}$ -GTP monomer and  $G_{\beta\gamma}$  dimer.  $G_{\alpha}$ -GTP monomer will start to interact with their intracellular proteins for signal transduction and will be discussed in below session (Walaas et al., 1992), whereas  $G_{\beta\gamma}$  dimer will tend to activate certain types of signaling molecules including ion channels,

lipid kinases, phospholipases as well as its own signaling cascades (Dorsam and Gutkind, 2007, Yuen et al., 2010).

#### **1.4.1 G<sub>q</sub>α protein-coupled receptors**

In vasculature, the activation of the G<sub>q</sub>α protein will cleave the phosphatidylinositol 4,5-bisphosphate (PIP<sub>2</sub>) into second messengers, inositol triphosphate (IP<sub>3</sub>) and DAG by binding its G<sub>q</sub>α-subunit to the phospholipase C (PLC). The IP<sub>3</sub> is soluble and diffusible in cell and binds to the intracellular receptor, IP<sub>3</sub> receptor (IP<sub>3</sub>R) which is located inside the cell and on the sarcoplasmic reticulum (SR) to trigger the intracellular release of the Ca<sup>2+</sup> ions from the SR into the cytosol. Whereas, the DAG will activate the PKC and result in the increase of Ca<sup>2+</sup> concentration in cytosol. In vasculature, the G<sub>q</sub>α protein-coupled receptors that are present in endothelium includes angiotensin-2 receptor (AT<sub>2</sub>), serotonin receptor (5-HT<sub>1D</sub>), bradykinin receptor (B<sub>2</sub>), muscarinic-3 receptor (M<sub>3</sub>), endothelin-B receptor (ET<sub>B</sub>R), and calcitonin receptor-like receptor (CALCRL). Whereas, there are α<sub>1</sub>-adrenergic receptor (α<sub>1</sub>), M<sub>3</sub> receptor, angiotensin-1 receptor (AT<sub>1</sub>), endothelin receptors (ET<sub>A</sub>R & ET<sub>B</sub>R), serotonin receptor (5-HT<sub>2</sub>), and thromboxane receptor (TXA<sub>2</sub>) present in VSMCs (Bockaert et al., 2006, Chen et al., 2000, de Gasparo et al., 2000, Goodman et al., 2001, Ishii and Kurachi, 2006, Jakala et al., 2009, Klabunde, 2011, Yildiz et al., 2013).

#### **1.4.2 G<sub>i</sub>α protein-coupled receptors**

In vasculature, there is a G<sub>i</sub>α protein-coupled receptor present in the VSMCs such as α<sub>2</sub>-adrenergic receptor (α<sub>2</sub>). Once this receptor is activated by its agonist, it will inhibit the activity of the cAMP-dependent AC to convert ATP into cAMP, hence causes vasoconstriction (Klabunde, 2011, Qin et al., 2008).

### **1.4.3 G<sub>s</sub>α protein-coupled receptors**

Typically, the G<sub>s</sub>α protein-coupled receptor is functionally opposed to G<sub>i</sub>α protein-coupled receptor, where it will activate AC to produce cAMP from ATP, the increase in the production of cAMP will subsequently enhance the activation of PKA and results in vasodilatory effect. There are at least two major G<sub>s</sub>α protein-coupled receptors present in VSMCs such as β<sub>2</sub>-adrenergic receptor (β<sub>2</sub>) and PGI<sub>2</sub> receptor (IP) (Jakala et al., 2009, Klabunde, 2011). In addition, the commonly used AC inhibitor for mechanism study is SQ22536 because it is more selective towards AC, higher cell-permeability and better solubility.

## **1.5 Channel-Linked Receptors**

These channels are also known as ion channel-linked receptors and/or ligand-gated receptors and/or ionotropic receptors. These receptors will be functionally activated when bound to its ligand and allowing ions such as sodium (Na<sup>+</sup>), potassium (K<sup>+</sup>), chloride (Cl<sup>-</sup>), and calcium (Ca<sup>2+</sup>) move through the membrane. In vasculature, the action potential which occurs in VSMCs will be regulated by these receptors through hyperpolarization or depolarization. There are two important channel-linked receptors playing major roles in vascular tone regulation which are K<sup>+</sup> channels and Ca<sup>2+</sup> channels.

### **1.5.1 Potassium channels (K<sup>+</sup>)**

K<sup>+</sup> channel is the most widely distributed types of ion channel in living organisms (Littleton and Ganetzky, 2000). Typically, there are four types of K<sup>+</sup> channels frequently discussed and investigated in vascular tone regulation which includes calcium-activated K<sup>+</sup> channel (K<sub>ca</sub>), voltage-gated K<sup>+</sup> channel (K<sub>v</sub>), ATP-sensitive K<sup>+</sup> channel (K<sub>ATP</sub>), and inwardly-rectifying K<sup>+</sup> channel (K<sub>ir</sub>).

### **1.5.1(a) Calcium-activated K<sup>+</sup> channel (K<sub>ca</sub>)**

In human vasculature, K<sub>ca</sub> channel can be further divided into three subtypes including big-conductance K<sub>ca</sub> channel (BK<sub>ca</sub>), intermediate-conductance K<sub>ca</sub> channel (IK<sub>ca</sub>), and small-conductance K<sub>ca</sub> channel (SK<sub>ca</sub>). BK<sub>ca</sub> channel is widely distributed in VSMCs, whereas IK<sub>ca</sub> and SK<sub>ca</sub> channels are abundantly expressed in endothelium (Ding et al., 2002, Eichler et al., 2003, Jakala et al., 2009, Marchenko and Sage, 1996). The electric conductance for BK<sub>ca</sub>, IK<sub>ca</sub>, and SK<sub>ca</sub> channels ranges between 100-300, 25-100, and 2-25 pS, respectively. In VSMCs, the BK<sub>ca</sub> channel is voltage and Ca<sup>2+</sup>-dependent, it will be activated by the increased intracellular Ca<sup>2+</sup> concentration, which allows the efflux of K<sup>+</sup> ions from the cytosol, hence creating hyperpolarization and the closure of the Ca<sup>2+</sup> channels, which results in vasodilatory effect (Feletou and Vanhoutte, 2005, Gautam et al., 2006). Furthermore, BK<sub>ca</sub> channel can be indirectly stimulated by the activation of PKA and PKG (Robertson et al., 1993, Scornik et al., 1993). IK<sub>ca</sub> and SK<sub>ca</sub> channels are slightly different from BK<sub>ca</sub> channel by which they are voltage-insensitive (Barfod et al., 2001, Hirschberg et al., 1998, Xia et al., 1998), but highly sensitive to the Ca<sup>2+</sup> and calmodulin concentration in cytosol (Garcia Pascual et al., 1995, Schumacher et al., 2001). The commonly used selective antagonist for BK<sub>ca</sub>, IK<sub>ca</sub>, and SK<sub>ca</sub> are iberiotoxin, clotrimazole, and apamin, respectively.

### **1.5.1(b) Voltage-activated K<sup>+</sup> channel (K<sub>v</sub>)**

In vasculature, the activation of K<sub>v</sub> channel is strictly dependent on the voltage changes across the membrane and is functionally correlated with the voltage-operated Ca<sup>2+</sup> channel (VOCC) in maintaining the membrane potential of VSMCs. K<sub>v</sub> channel will reverse the depolarizing state of the membrane potential back to steady state (Nelson and Quayle, 1995). Typically, there are two major subunits for K<sub>v</sub> channel

which are the alpha subunits, which can be further grouped into 12 subclasses, and the beta subunits. They are functionally activated to hasten the efflux of  $K^+$  from the cytosol out to the exterior, hence a more rapid increase of repolarizing current, with less activation of  $Ca^{2+}$  channels (Jakala et al., 2009, Robertson and Nelson, 1994, Yildiz et al., 2013). In addition, the cAMP-dependent PKA can indirectly increase the amplitude of the  $K_v$  currents (Aiello et al., 1995) and inhibited by the activation of PKC (Cole et al., 1996). The commonly used inhibitor for its mechanism study is 4-aminopyridine (4-AP).

#### **1.5.1(c) Inwardly-rectifying $K^+$ channel ( $K_{ir}$ )**

This channel contains pore domain which is homologous to  $K_v$  channel, and therefore it has been classified as one of the member in  $K_v$  channel. The  $K_{ir}$  channel needs to bind with  $PIP_2$  to be activated, and functionally prefer the inward flow of the  $K^+$  ions rather than outward, hence hastening the recovery of the membrane potential back to resting state (Feletou and Vanhoutte, 2005, Ganong, 1993, Tucker and Baukowitz, 2008). The activation of this channel in endothelium will contribute as EDHFs for inducing the relaxing of VSMCs (Edwards et al., 1998). The only different of  $K_{ir}$  channel compared to other  $K^+$  channels is it will only be activated when the membrane potential has reached hyperpolarization state, then allowing the influx of  $K^+$  ions into the cytosol to reach resting potential (Edwards and Weston, 1995). The only selective antagonist used for the  $K_{ir}$  channel study is barium chloride ( $BaCl_2$ ).

#### **1.5.1(d) ATP-sensitive $K^+$ channel ( $K_{ATP}$ )**

This channel will be activated by increasing intracellular ADP and decreasing intracellular ATP, also called ATP-sensitive channel and is located in VSMCs (Ashcroft and Ashcroft, 1990, Boyd et al., 1990, Ko et al., 2008, Standen et al., 1989). In resting potential,  $K_{ATP}$  channel acts as a weak inwardly rectifying  $K^+$  channel, thus it was

classified as a member in  $K_{ir}$  channel family. However, once  $K_{ATP}$  channel is activated, it will produce  $K^+$  efflux from the cytosol to maintain a negative resting potential, hence causing vasodilatory effect (Jakala et al., 2009). The commonly used selective  $K_{ATP}$  channel inhibitor for mechanism study is glibenclamide.

### **1.5.2 Calcium channels ( $Ca^{2+}$ )**

The  $Ca^{2+}$  ion-linked receptor is selectively permeable for  $Ca^{2+}$  ions and allows its entrance into the cytosol, hence creates depolarization, and induces vasoconstriction. Typically, there are two different types of  $Ca^{2+}$  channel such as VOCC and receptor-operated  $Ca^{2+}$  channels (ROCC). Generally, there are two ways to increase the cytosolic  $Ca^{2+}$  concentration which are through 1) the influx of  $Ca^{2+}$  ions from exterior or 2) intracellular release of  $Ca^{2+}$  from the SR store.  $Ca^{2+}$  ion is one of the most crucial second messengers in vascular tone regulation. The intracellular increase of  $Ca^{2+}$  concentration will cause membrane depolarization and allow the up-regulation of  $Ca^{2+}$ -calmodulin complexes. In the cross-bridge cycle in VSMCs, the activated calmodulin will stimulate the MLC kinases (MLCK) to phosphorylate the MLC at serine residue-19 to form a cross-bridge with the actin filament, and again form actin-myosin protein (AMP), hence causes the VSMCs contraction via the sliding filament mechanism (Gao et al., 2003, Jakala et al., 2009, Marchenko and Sage, 1996, Webb, 2003). In addition, there is another enzyme in this cross-bridge, the MLC phosphatases (MLCP) which can dephosphorylate the MLC in order to terminate the smooth muscle contraction.

#### **1.5.2(a) Voltage-operated $Ca^{2+}$ channel (VOCC)**

In vasculature, VOCC is one of the most important receptors used to control the vascular tone by maintaining the membrane potential of the VSMCs. Here, the VOCC is normally referred to as the L-type  $Ca^{2+}$  channel that is in VSMCs. In normal

physiological condition, the concentration of the  $\text{Ca}^{2+}$  ions outside the cell is around 3-4 mM which is thousand-fold compare to inside the cell, which is normally kept at or below 100nM (McFadzean and Gibson, 2002). Therefore, once the membrane potential reached depolarization stage, the  $\text{Ca}^{2+}$  ions will rush into the cytosol from the outside via VOCC, hence results in vasoconstriction (Goodman et al., 2001).It is functionally correlated with  $\text{K}_v$  channel in controlling the membrane potential. The commonly used antagonist for this channel mechanism study is nifedipine due to its highly vascular selectivity (Furberg et al., 1995).

### **1.5.2(b) Receptor-operated $\text{Ca}^{2+}$ channel (ROCC)**

The calcium cannot only enter the VSMCs by  $\text{Ca}^{2+}$  influx via VOCC, but also through intracellular  $\text{Ca}^{2+}$  release via the ROCC that could lead to the membrane depolarization (Berridge, 1997, Gibson et al., 1998). The ROCC normally refer to certain members of GPCRs that are capable of inducing the intracellular release of  $\text{Ca}^{2+}$  ions from the SR store into the cytosol by producing its second messenger (Landsberg and Yuan, 2004, McFadzean and Gibson, 2002). Typically, there are at least three types of receptors that are categorized as ROCC such as  $\text{IP}_3\text{R}$ , RyRs, and store-operated  $\text{Ca}^{2+}$  channels (SOCC).

#### **1.5.2(b)(i) Inositol triphosphate receptor ( $\text{IP}_3\text{R}$ )**

The  $\text{IP}_3\text{R}$  is located on the surface of the SR, which will be activated by the second messenger,  $\text{IP}_3$  that is produced by activated  $\text{G}_q\alpha$  protein-coupled receptors. It is the main site for the intracellular  $\text{Ca}^{2+}$  release from the SR store into the cytosol which leads to an increase in the formation of  $\text{Ca}^{2+}$ -calmodulin complexes (Putney et al., 2001). Regarding to this mechanism study, the selective  $\text{IP}_3\text{R}$  blocker, 2-aminoethoxydiphenyl borate (2-APB) is commonly used.

### **1.5.2(b)(ii) Ryanodine receptor (RyRs)**

This receptor is less likely distributed in vascular, however, it plays minor role in controlling the intracellular release of  $\text{Ca}^{2+}$  ions into the cytosol by using calcium-induced calcium release (CICR). The increasing  $\text{Ca}^{2+}$  ions concentration in cytosol will trigger the RyRs to release more  $\text{Ca}^{2+}$  ions from the SR store which subsequently causes a transient  $\text{Ca}^{2+}$  spark, which is important for muscle contraction.

### **1.5.2(b)(iii) Store-operated $\text{Ca}^{2+}$ channel (SOCC)**

The primary function of SOCC is to refill  $\text{Ca}^{2+}$  ions, and it is known as capacitative-dependent calcium entry channel whereby its activation across the plasma membrane will occur with the depletion of the  $\text{Ca}^{2+}$  stores (Feletou and Vanhoutte, 2005, McFadzean and Gibson, 2002). The sacro/endoplasmic reticulum  $\text{Ca}^{2+}$ -ATPase (SERCA) is the only specialized pumps used to transport the  $\text{Ca}^{2+}$  ions from the extracellular into the SR store to re-accumulate the calcium concentration back to the range between 0.5-1 mM. In the SR store, the  $\text{Ca}^{2+}$  ions will bind to calsequestrin with the purpose of decreasing the free mobile  $\text{Ca}^{2+}$  ions in the SR, hence more calcium can be stored (Chemaly et al., 2013, Swietach et al., 2008, Wood, 2016). The selective SOCC blocker, gadolinium ( $\text{Gd}^{3+}$ ) is usually accompanied with the use of the selective blocker of SERCA, thapsigargin (Rogers et al., 1995) during the mechanism study of SOCC pathway.

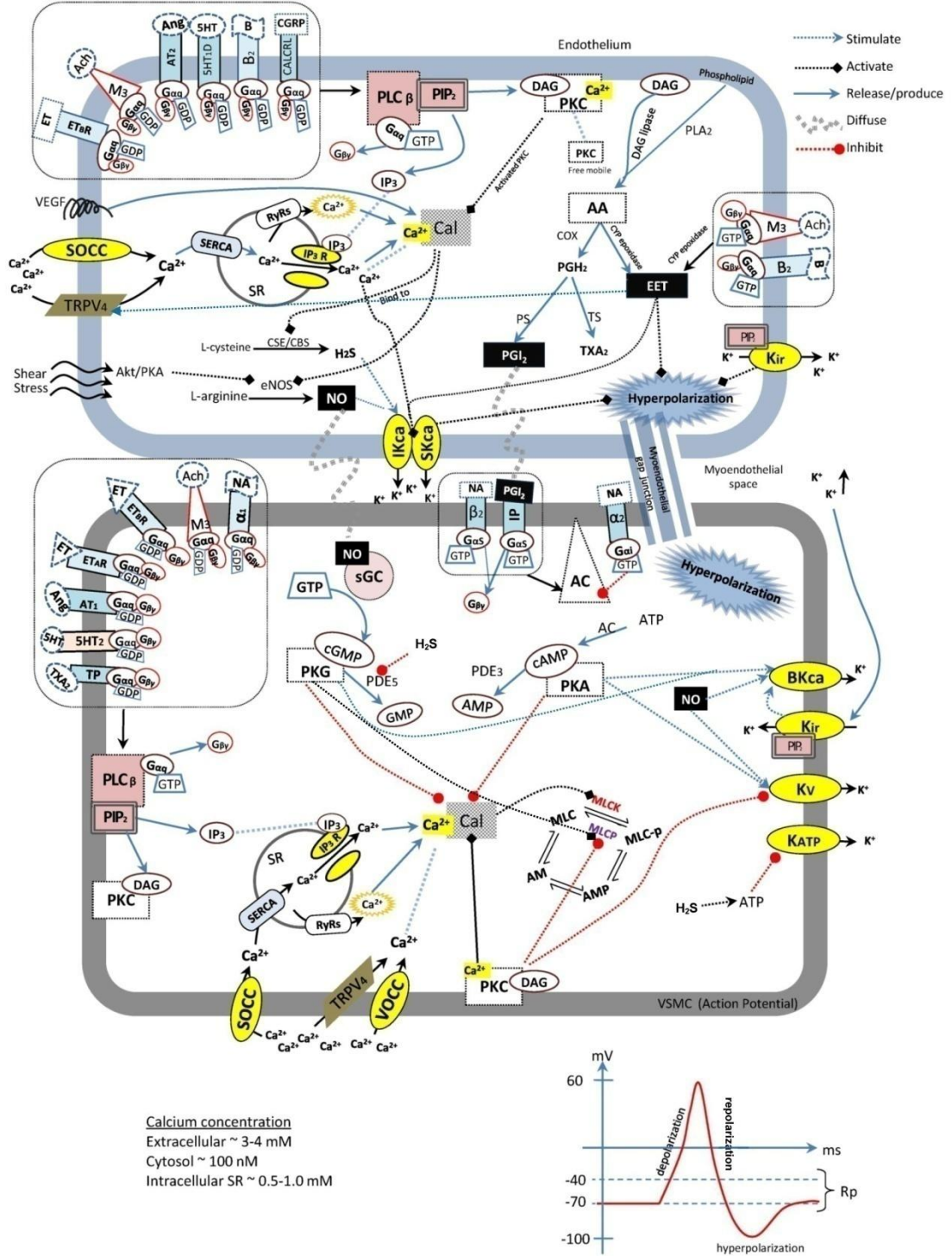


**Figure 1.1:** Overall signaling mechanism pathways that happen in vascular endothelium and vascular smooth muscle cells which mediate vascular tone regulation.

In summary, there are plenty of signaling mechanism pathways mediating vascular tone regulation as shown in Figure 1.1. However, in the signaling mechanism studies of vasodilatory effect of drugs, there are a few major vasodilation-predominated signaling pathways that need to be studied and investigated such as NO, PGI<sub>2</sub>, sGC, cGMP, muscarinic receptors,  $\beta_2$ -adrenergic receptors, K<sub>ca</sub>, K<sub>v</sub>, K<sub>ir</sub>, K<sub>ATP</sub>, VOCC, and IP<sub>3</sub>R. According to the literature, all these pathways were frequently studied in the *in vitro* antihypertensive pharmacological research related to vasculature (Loh et al., 2016, Rameshrad et al., 2016). All these signaling mechanism studies have been included in this thesis as well.

## **1.6 Problem Statements**

Despite there are varieties of synthetic antihypertensive drugs available in the current market, there are often many scientific reports on their relatively low efficacies in term of monotherapy as well as undesired chronic adverse effects (Düsing, 2010). According to the trend of antihypertensive drugs evolution, the classes of antihypertensive drugs used clinically often changes from year-to-year with the purpose of achieving the targeted blood pressure range. For instance, the development of antihypertensive drugs have evolved in such an order: Rauwolfia alkaloid, reserpine, thiazides,  $\beta$ -blockers, calcium-channel blockers (CCBs),  $\alpha$ -blockers, angiotensin-converting-enzyme inhibitor (ACEI), angiotension II-receptor blockers (ARBs), and direct renin inhibitor (DRI) Aliskiren. However, according to the Clinical Practice Guidelines in Management of Hypertension (4<sup>th</sup> edition) in Malaysia, the favored choice of first line monotherapy has included only five classes from the aforementioned including ACEI, ARBs, CCB, diuretic-thiazide, and  $\beta$ -blockers, and report stated that only 35% of the patients' blood pressure was successfully controlled by treatment (MOH, 2013). Therefore, combination

therapy is often preferred and was claimed to be more effective in achieving the target blood pressure. At the same time, approximately 60% of the hypertensive patients in Europe countries require  $\geq 2$  antihypertensive agents to reach the desired blood pressure (MOH, 2013). Because of this, the US, European Society of Hypertension (ESH) and European Society of Cardiology (ESC) guidelines have provided a few options for two drugs combinations such as the combination of diuretic with either CCBs or ACEI/ARBs, while only a single remedy for three drugs combination such as ACEI/ARBs with CCBs plus a diuretic (Düsing, 2010). Thus, the discovery of new antihypertensive drugs is still a hot topic in the field of pharmaceutical research.

From the perspective of traditional Chinese medicine (TCM), it employs a syndromatic treatment system which treats diseases based on its syndromes. Based on the principles of TCM, hypertension is a multi-syndromic disease that is caused by phlegm fluid retention, fire, and deficiencies syndromes. The first syndrome is fire syndrome that could further categorized into four types such as liver fire, heart fire, stomach fire or intestine fire. The second syndrome is the phlegm-fluid retention syndrome. The third syndrome is deficiency syndrome that normally happens in the spleen or the kidney (Qian et al., 2003, Wang and Xiong, 2013). Since ancient times, TCM herbs have been shown to be capable of providing extraordinary therapeutic effect in the treatment of hypertension based on their holistic benefits along with insignificant arise of safety concern. Moreover, the combination of TCM herbs could possibly enhance the therapeutic effect of the main herb in eliciting its vasodilatory effect. These phenomena could be attributed to the variety of vasoactive components present in the combined TCM herbs, which could tackle hypertension through multiple signaling mechanism pathways simultaneously.

In this study, five TCM herbs that are frequently used as clinical prescriptions to counteract different syndromes caused by the hypertension which includes *Gastrodia elata*, *Uncaria rhynchophylla*, *Pueraria thomsonii*, *Panax notoginseng*, and *Alisma orientale* were selected for antihypertensive drugs research by using orthogonal stimulus-response compatibility group studies with  $L_{25} (5^5)$  formulation. The high performance thin layer chromatography (HPTLC) and Fourier transform infrared (FTIR) spectroscopy identification methods were used to authenticate the fingerprints of the five herbs by comparison to their respective marker compounds before the experiments started. The vasodilatory effects of formulated combined herbs were determined by using *in vitro* aortic rings assay, followed by oral administration to the spontaneous hypertensive rats (SHRs) for 28 days consecutively in different dosages along with toxicology study. The formulated combined herbs was expected to exert strongest vasodilatory effects using holistic mechanism of actions compared to single herbal extract, as well as to exhibit a strong antihypertensive effects in *in vivo* whilst without causing adverse effect in animal models.

### **1.7 Objectives**

The main objectives of present study were

- a) To investigate the vasodilatory effects of the most potent extracts from *G. elata*, *U. rhynchophylla*, *P. thomsonii*, *P. notoginseng*, and *A. orientale* using *in vitro* aortic rings assay.
- b) To determine the optimum ratio of combining five most potent solvent extracts from five TCM herbs by using  $L_{25} (5^5)$  formulation orthogonal stimulus-response compatibility group studies (named as F1).

- c) To determine the most suitable solvent to extract *U. rhynchophylla*, *P. thomsonii*, *P. notoginseng*, and *A. orientale* that prepared in optimized ratio (F1) to exert the highest vasodilatory effect using *in vitro* aortic rings assay.
- d) To study the mechanism of action of vasodilatory effects for the ratio optimized combination of five TCM herbs (F1-2) using *in vitro* aortic rings assay, and partial characterization on its vasoactive components using tri-step Fourier transform infrared spectroscopy and high performance thin layer chromatography.
- e) To determine the antihypertensive and toxicity effects of F1-2 via *in vivo* study on spontaneous hypertensive rats.

## CHAPTER 2

# HERBAL AUTHENTICATION USING HIGH PERFORMANCE THIN LAYER CHROMATOGRAPHY AND TRI-STEP FOURIER TRANSFORM INFRARED SPECTROSCOPY

### 2.1 Introduction

As aforementioned, the five TCM herbs which include *G.elata*, *U. rhynchophylla*, *P. thomsonii*, *P. notoginseng*, and *A. orientale* were selected for this antihypertensive drug research based on their own capability to cure the specific syndromes caused by the hypertension. Before the experiment carried put, the authenticity of the five purchased raw herbs was assured macroscopically upon purchasing from the local medical hall by the TCM's expert, Dr. Yam Mun Fei. After that, the fingerprints of five herbs were identified by using high performance thin layer chromatography (HPTLC) and tri-step Fourier transform infrared (tri-step FTIR) spectroscopy methods.

#### 2.1.1 High-performance thin layer chromatography (HPTLC)

Basically, all herbs may contain highly complex mixtures of compounds that cover a wide range of substance classes and they are used to exhibit natural variability. Therefore, the choice of selecting an appropriate analytical method is crucial in order to achieve highly reliable and reproducible results, both in qualitative and quantitative manners. HPTLC fingerprint is one of the ideal analytical methods that can be used to identify the complex herbal entities (Sai Saraswathi et al., 2017). Fundamentally, HPTLC is the improved form of TLC, by using the same principles, the mobile phase promotes the separation of compound mixtures by differential migration according to

their polarity across the stationary phase, subsequently the TLC plate will be examined under UV light with different wavelength and the distances travelled by the separated substances will be calculated as retention factor ( $R_f$ ). However, HPTLC provides extra credits by providing enormous flexibility in the selection of the parameters for different analysis, enhanced resolution, automation steps, and highly accurate quantitative measurements. HPTLC is known as a powerful and rapid analytical tool due to its high flexibility, precision, and accuracy (Maldini et al., 2016). The automation steps of the HPTLC has tremendously enhanced the reproducibility of the quantitative results, and thus it was proposed to be included in various pharmacopeia (Gün et al., 2014, John et al., 2015, Motisariya et al., 2013, Pikul et al., 2013). In this section, the HPTLC fingerprints of each raw herb were compared to the fingerprints of their standard herbs that were purchased from National Institutes for Food and Drug Control, China, as well as compared with their marker compounds that were purchased from Chengdu Biopurify Phytochemicals Ltd, Sichuan, China in order to prove the authenticity of the raw herbs.

### **2.1.2 Tri-step Fourier transform infrared spectroscopy (tri-step FTIR)**

The principles applied in tri-step FTIR is same with FTIR whereby it measures the infrared radiation absorbed or emitted by the substances which normally appears in mid-IR ( $5000-400\text{ cm}^{-1}$ ) or near-IR region ( $10000-4000\text{ cm}^{-1}$ ), and rarely in far-IR region ( $200\text{ cm}^{-1}$ ), and the resulting absorption peak appeared in the spectrum corresponds to the bonds present in the molecules of the substances. Tri-step FTIR consists of three types of identifications methods such as conventional FTIR (1D-IR), second-derivative IR (SD-IR), and 2D-correlation IR (2D-IR) spectroscopy. Tri-step FTIR is easy and rapid, and is used to provide highly reproducible fingerprint results which make it the golden identification method in determining the authenticity of TCM materials. The

main advantage of tri-step FTIR is that the sample does not need to undergo any destructive chemical or physical perturbation processes such as fractionation which could cause the original samples to behave differently, and therefore the most complete and true information among the relationship between different chemical compounds in each herb can be obtained (Sun et al., 2011).

During the spectra interpretation, some of the characteristic peaks would be too small due to the low concentration of a particular chemical constituent within the sample, or had been unintentionally masked by bigger peaks, thus those peaks were invisible for interpreting in the 1D-IR spectra. Therefore, the SD-IR spectroscopy with its higher resolution can be used to solve this problem by emphasizing the hidden peaks in the SD-IR spectra (Sun et al., 2003). Moreover, the 2D-IR spectroscopy is the next step to compensate the drawbacks of other analytical systems by exposing the samples to external perturbation, and therefore altering the intra- and intermolecular relationship of the chemical constituents within the samples. Subsequently, the relationship between functional groups could be analyzed from the dynamic spectra obtained (Li et al., 2014, Li et al., 2015). In this section, the 1D-IR spectra of raw herbs were compared to the standard herbs that were purchased from National Institutes for Food and Drug Control, China to prove their authenticity.

## **2.2 Methodology**

### **2.2.1 Herbs and chemicals**

The *G. elata*, *U. rhynchophylla*, *P. thomsonii*, *P. notoginseng*, and *A. orientale* raw herbs were purchased from the local medical hall and macroscopically authenticated by the expert of TCM, Dr. Yam Mun Fei. The *G. elata*, *U. rhynchophylla*, *P.lobata*, *P. notoginseng*, and *A. orientale* standard herbs were purchased from National Institute for

Food and Drug Control (Beijing, China). The marker compounds such as gastrodin, rhynchophylline, isorhynchophylline, puerarin, ginsenoside Rb1, ginsenoside Rg1, and alisol B acetate were purchased from Chengdu Biopurify Phytochemicals Ltd (Sichuan, China). HPTLC 60G F<sub>254</sub> plate and potassium bromide (KBr) were bought from Merck (Germany). Chloroform, ethyl acetate, formic acid, petroleum ether, and ethanol were purchased from QReC (New Zealand). Methanol was purchased from J. T. Baker (USA).

### **2.2.2 High performance thin layer chromatography**

All samples were freshly prepared on the day of analysis. *G. elata*, *U. rhynchophylla*, *P. thomsonii*, *P. notoginseng*, and *A. orientale* raw and standard herbs were prepared in concentration of 100 mg/ml by dissolving in methanol separately. The marker compounds preparations for each herb were described at 2.2.2(a)-(e). After that, all the samples were centrifuged at 3500 rpm for 15 min at room temperature, and the supernatant was transferred into vials prior to analysis. These experiments were carried out by using the HPTLC developed by CAMAG which is equipped with the automatic developing chamber (ADC 2), automatic TLC sampler 4 (ATS 4), TLC visualizer, and TLC scanner 4. All data were interpreted by using VisionCATs software version 2.2.16187.4 (CAMAG, Muttenz, Switzerland).

2 µl of each sample were applied as 8 mm width bands with 11.4 mm distance between bands on 20 X 10 cm HPTLC plate. The bands were applied at 8 mm distance from the bottom edge, and 20 mm distance from left edge. Methanol was used to rinse the spotting needle for three cycles when different samples were applied. The samples spotted TLC plate was transferred to ADC 2 which is equipped with a 20 X 10 cm twin-through chamber containing 25 ml of mobile phase for saturation, and another 10 ml for development. Before the mobile phase developments, the chamber was saturated for 10